Supporting Information

Measuring DNA hybridization kinetics in live cells using a time-resolved 3D single-molecule tracking method

Yuan-I Chen[1], Yin-Jui Chang[2], Trung Duc Nguyen[1], Cong Liu[1], Stephanie Phillion[1], Yu-An Kuo[1], Huong T. Vu[1], Angela Liu[1], Yen-Liang Liu[1], Soonwoo Hong[1], Pengyu Ren[1], Thomas E. Yankeelov [1,4,5,6,7], and Hsin-Chih Yeh[1,3]*

[1]Department of Biomedical Engineering, University of Texas at Austin, Austin, TX, USA

[2]Department of Mechanical Engineering, University of Texas at Austin, Austin, TX, USA

[3]Texas Materials Institute, University of Texas at Austin, Austin, TX, USA

[4]Oden Institute for Computational Engineering and Sciences, University of Texas at Austin, Austin, TX, USA

[5]Department of Diagnostic Medicine, University of Texas at Austin, Austin, TX, USA

[6]Department of Oncology, University of Texas at Austin, Austin, TX, USA

[7]Livestrong Cancer Institutes, University of Texas at Austin, Austin, TX, USA

Contents:

I. Materials and Methods

1. 3D SMT microscope. The 3D SMT system is built around customized Olympus IX-71 microscope. The 640 nm pulsed laser (PicoQuant LDH-P-C-640B) is reflected by the dichroic mirror (Semrock FF650-Di01-25x36), and focused by a 60X NA=1.2, water immersion objective (Olympus, UPLSAPO60XW). The Keplerian beam expander controls the laser beam size for the slightly underfilling the objective. The single dye is excited by the 640 nm laser and fluorescence is collected by the same 60X water immersion objective, and then filtered by ET700/75 m (Chroma). Based on the number of photons collected through two optical fiber bundles (Polymicro, 50-μm core diameters, 55-μm center-to-center spacing) in every 5 ms, xyz piezo stage (PI, P-733K130) is used to reposition the fluorescent molecule to the center of excitation focus with 30×30×30 μm travel range. In other words, four barely overlapped confocal volumes are created in the sample space (red and blue oval balls), each corresponding to the front end of four multimode optical fibers that connect to four APDs. The two fiber bundles (red and blue) are orthogonally installed and slightly offset along the optical axis ($I_A \neq I_B$), giving the four confocal volumes a "tetrapod" geometry in the sample space. The system is controlled by LabVIEW (**Supplementary Fig. 2**). A spinning disk unit (CrestOptics) is also integrated with the 3D-SMT system (with Andor EMCCD camera).

2. Error Signal Analysis as Feedback Control Algorithm. Our confocal-feedback 3D-SMT system employs Error Signal Analysis for our feedback control system to estimate the xyz position of the target molecule. Given the differences in photon counts collected by single-photon counting modules (I_1, I_2, I_3, I_4), the molecular position is determined by the following equations:

$$\Delta x = k_x \frac{I_1 - I_2}{I_1 + I_2} \quad \text{Equation S2.1}$$

$$\Delta y = k_y \frac{I_3 - I_4}{I_3 + I_4} \quad \text{Equation S2.2}$$

$$\Delta z = k_z \frac{(I_1 + I_2) - (I_3 + I_4)}{(I_1 + I_2) + (I_3 + I_4)} \quad \text{Equation S2.3}$$

where, k_x, k_y, k_z are the proportional gains for each dimension respectively. An active feedback control based on the molecular position is then used to drive the xyz piezo stage and keep the molecule located at the center of the confocal volumes. With the motion history of the piezo stage, the 3D trajectory of the molecule is obtained with the tracking range $\pm 15\mu m$ in three dimensions.

3. Antibunching. Fluorescence antibunching is a unique property that enables us to determine the number of emitters contributing to a ray of light[1]. A single molecule that is in the ground state can be excited by laser light, and then resides in the excited state until it returns to the ground state by the emission of a photon. Subsequently, the molecule may undergo the next excitation–emission cycle. Evidence has shown that photons can only be emitted one at a time within this process. In other words, the probability to observe a photon after the detection of a previous one vanishes as the time interval between the photon-pair approaches zero. Antibunching behavior exists only when the molecule is a single quantum emitter. Here we have utilized this property as the ultimate proof that a single fluorescent molecule is tracked by our system. By virtue of the single-photon counting detector and time-correlated single-photon counting module (TCSPC; PicoHarp 300), we can perform antibunching analysis of the tracked molecule. From our time-tag-time-resolved data from TCSPC module, we can extract every single trajectory and perform antibunching analysis to confirm the trajectory belong to a single-molecule fluorescence. The time difference between two photons detected by the transmission channel and the reflection channel is repeatedly measured and histogrammed with 128 ps resolution.

4. Fluorescence lifetime fitting with maximum likelihood estimation. In TCSPC module, the observed fluorescence lifetime histogram c_i is given by the following equation.

$$c_i(\tau, s) = IRF \otimes (e^{-t/\tau}) \quad \text{Equation S4.1}$$

where IRF represents the instrument response function, τ is the fluorescence lifetime, and s is the shift of the IRF with respect to the fluorescence decay.

The reduced $2I_r^*$ for maximum likelihood estimation is obtained by normalizing negative of log-likelihood, $2I^*$, by the degree of freedom $(k - 1 - f)$,

$$2I_r^* = \frac{2}{k-1-f} \sum_{i=1}^{k} n_i \ln\left(\frac{n_i}{Sm_i(\tau, s, \gamma)}\right) \quad \text{Equation S4.2}$$

where the total signal counts S are assumed to be accumulated in k bins in TCSPC, n_i represents the number of the detected photons in i^{th} bin, f is the number of the fitted parameter, and m_i represents the probability of that a photon will fall into channel i, which is given by the equation as follows,

$$m_i(\tau, s, \gamma) = \frac{\gamma^2}{k} + (1-\gamma^2)\frac{c_i(\tau,s)}{\sum c_i(\tau,s)} \quad \text{Equation S4.3}$$

where γ^2 represents the fraction of the constant background. The value of s and γ are determined by minimizing $2I_r^*$ during the calibration experiment. Those two determined values stay constant in the further analysis, which means that there is only a changeable parameter of interest τ. To ensure good signal-to-noise ratio and accurate estimations, the fluorescence decays of all the channels are added up for the integration analysis.

5. Hidden Markov Model analysis on FRET phenomenon. The Hidden Markov Model (HMM) has been developed for several fields such as temporal pattern recognition, including speech, gesture recognition, musical score following, and bioinformatics, which includes the analysis of ion-channel data and the single-molecule fluorescence data as well. A Markov process, also known as Markov chain, represents a sequence of the state-to-state transition with the kinetics parameters controlled by single-exponential decay. It has been demonstrated better than dwelling time analysis since the underlying process is hidden in the data due to the noise. Given a sequence of observations (each number representing the lifetime value measured at a given time), HMM was performed to find the "hidden" sequence of states (binding or unbinding) which caused such observations. In our experiment, the phenomenon of FRET with two "digital" states can be observed from the lifetime traces. The transition between two disparate states (binding/unbinding) is analyzed by ebFRET, a MATLAB library for single-molecule FRET signals analysis with a hidden Markov Model, yielding the transition matrix p_{11}, p_{12}, p_{21}, p_{22}. The transition matrix is further employed to determine the hybridization kinetics. ebFRET provides an advantage to discern the kinetics with average dwelling time shorter than the temporal resolution of the lifetime traces or longer than the average track duration (116 ms *in vitro* and 105 ms *in vivo*).

6. From HMM transition matrix to apparent annealing/melting rate. A Hidden Markov Model has been used to model two-state single-molecule tracks. In our case, the unbinding (melted) state is represented as state 1, whereas the binding (hybridized) state is represented as state 2. The state transition matrix p_{ij} $(i, j \in [1, 2])$ indicates the probability of the transitioning from state i to state j in one step. A proper conversion from the estimated transition matrix reported by ebFRET to the apparent annealing (k'_{on}) and the melting rate (k_{off}) of interest is performed by the following equations:

$$p_{12} = \frac{\acute{k_{on}}}{\acute{k_{on}}+k_{off}}[1 - e^{-(\acute{k_{on}}+k_{off})\Delta t}] \quad \text{Equation S6.1}$$

$$p_{21} = \frac{k_{off}}{\acute{k_{on}}+k_{off}}[1 - e^{-(\acute{k_{on}}+k_{off})\Delta t}] \quad \text{Equation S6.2}$$

$$p_{11} = 1 - p_{12} \ , p_{22} = 1 - p_{21} \quad \text{Equation S6.3}$$

$$\acute{k_{on}} = -\frac{p_{12}\ln(1-p_{21}-p_{12})}{(p_{12}+p_{21})\Delta t} \quad \text{Equation S6.4}$$

$$k_{off} = -\frac{p_{21}\ln(1-p_{21}-p_{12})}{(p_{12}+p_{21})\Delta t} \quad \text{Equation S6.5}$$

The standard deviation of estimated $\acute{k_{on}}$ and k_{off} can be obtained via the following equations:

$$Std\left(\acute{k_{on}}\right) = \sqrt{\left(\frac{\partial \acute{k_{on}}}{\partial p_{12}}\right)^2 Std(p_{12}) + \left(\frac{\partial \acute{k_{on}}}{\partial p_{21}}\right)^2 Std(p_{21}) + 2\left(\frac{\partial \acute{k_{on}}}{\partial p_{12}}\right)\left(\frac{\partial \acute{k_{on}}}{\partial p_{21}}\right) Cov(p_{12}, p_{21})} \quad \text{Equation S6.6}$$

$$Std(k_{off}) = \sqrt{\left(\frac{\partial k_{off}}{\partial p_{12}}\right)^2 Std(p_{12}) + \left(\frac{\partial k_{off}}{\partial p_{21}}\right)^2 Std(p_{21}) + 2\left(\frac{\partial k_{off}}{\partial p_{12}}\right)\left(\frac{\partial k_{off}}{\partial p_{21}}\right) Cov(p_{12}, p_{21})} \quad \text{Equation S6.7}$$

$$Cov(p_{12}, p_{21}) = 0 \quad \text{Equation S6.8}$$

where,

$$\frac{\partial k_{on}^{'}}{\partial p_{12}} = -\frac{p_{12}(p_{12}+p_{21})+p_{21}(p_{12}+p_{21}-1)\ln(1-p_{12}-p_{21})}{\Delta t(p_{12}+p_{21}-1)(p_{12}+p_{21})^2} \quad \text{Equation S6.9}$$

$$\frac{\partial k_{on}^{'}}{\partial p_{21}} = \frac{p_{12}((p_{12}+p_{21}-1)\ln(1-p_{12}-p_{21})-p_{12}-p_{21})}{\Delta t(p_{12}+p_{21}-1)(p_{12}+p_{21})^2} \quad \text{Equation S6.10}$$

$$\frac{\partial k_{off}}{\partial p_{12}} = \frac{p_{21}((p_{12}+p_{21}-1)\ln(1-p_{12}-p_{21})-p_{12}-p_{21})}{\Delta t(p_{12}+p_{21}-1)(p_{12}+p_{21})^2} \quad \text{Equation S6.11}$$

$$\frac{\partial k_{off}}{\partial p_{21}} = -\frac{p_{21}(p_{12}+p_{21})+p_{12}(p_{12}+p_{21}-1)\ln(1-p_{12}-p_{21})}{\Delta t(p_{12}+p_{21}-1)(p_{12}+p_{21})^2} \quad \text{Equation S6.12}$$

7. Simulation of Hidden Markov Model analysis by ebFRET algorithm. The ebFRET algorithm[2] is benchmarked by the simulated lifetime traces generated *in silico*.

$$\tau(t_i) = \begin{cases} y \sim N(\tau_B, \sigma_B^2), & if\ \ s(t_i) = binding\ \ state \\ y \sim N(\tau_U, \sigma_U^2), & if\ \ s(t_i) = unbinding\ \ state \end{cases} \quad \text{Equation S7.1}$$

where τ_B (1.6 ns) and τ_U (2.6 ns) are the constants obtained from our *in-vivo* experimental data when the quencher strand concentration is 1.15** nM (Asterisk (**) means estimated concentration), $s(t_i)$ represents the state of the tracked molecule at time t_i. σ_B^2, σ_U^2 are the variance of fluorescence lifetime estimation determined to be 11% based on the experimental parameters.

The transition rates, k'_{on} and k_{off}, were assumed to be 5 and 10 s^{-1}, respectively, for Monte Carlo simulation. The tracking durations of the simulated trajectories follow the geometric distribution:

$$p(x = k\Delta t) = (1-p)^{k-1}p \quad \text{Equation S7.2}$$

where *1-p* represents the probability of successful tracking in each time step, and the tracking of single-molecule was assumed to be a sequence of Bernoulli trails. *p* is determined to be 0.11 from our *in-vivo* experimental data. Eventually, given k'_{on}, k_{off}, 15 ms as Δt, the time series of the states $s(t_i)$ was generated by MATLAB package pmtk3, representing as a Markov chain for Hidden Markov Model analysis.

8. Discrepancies between 3D-SMT kinetics results and surface kinetics. In literature, we have seen single-molecule mechanical studies (on a surface) give extrapolated zero-force k_{off} values that were 100-10,000x different from the fluorescence-based estimate (in solution)[3] , which could be a surface effect. Even with a well passivated surface, many factors (such as how DNA is tethered to the surface[4], how proximal DNA is to the surface, and how dense DNA is on the surface) can still alter the hybridization equilibria and kinetics[5], leading to results that are quite different from the solution-based measurements. Electrostatic interactions have also been shown to influence the stability of surface-tethered duplexes[6-7]. In addition, both hydrophobicity of the surrounding surface[8] and reduction in conformational freedom of tethered ssDNA[9] favor single-strand hairpin formation, thus reducing duplex stability. But we do not have any of these problems in our 3D-SMT method. Our method is truly one-of-a-kind – we can actively track a NA molecule freely diffusing in solution while simultaneously measure the hybridization kinetics on the same molecule. While we are indeed studying the hybridization behaviors of short sequences, we are the only group to do this "at the single-molecule level" and "inside live cells".

We also want to emphasize that k_{on} measured by surface-based methods are expected to be slower than those measured in solution due to the restricted motion of the immobilized probes on the surface, which reduces collision frequencies compared to a reaction in solution (where both probe and target are freely diffusing)[10-11]. But we do not often see a head-to-head comparison for surface-based methods and solution-based method (exactly identical DNA probe design, fluorophore, and ionic strength). The reason that our k_{on} values are 1.5 to 3-fold higher than those measured by surface-based single-molecule techniques (such as k_{on} from Nesbitt's[12], Harris'[10] and Simmel's[13] groups) could be simply due to the higher collision frequencies[2, 10]. But all surface-related effects, sequence difference and ionic strength difference need to be considered when making a fair comparison.

9. Non-linear and non-monotonic relationship between melting temperature T_m and k_{on} and k_{off}. T_m is not an intrinsic property of the DNA molecule itself, but rather depends on the DNA concentration. At melting temperature,

$$\Delta G^0 = \Delta H^0 - T_m \Delta S^0 = -RT_m \ln(\frac{c}{2}) \quad \text{Equation S9.1}$$

$$T_m = \frac{\Delta H^0}{\Delta S^0 - R\ln(\frac{c}{2})} \quad \text{Equation S9.2}$$

where *c* is the concentration of the DNA. However,

$$\frac{k_{on}}{k_{off}} = e^{-\Delta G^0/RT} \quad \text{Equation S9.3}$$

As we can see here, there is no causative relationship between T_m, k_{on} and k_{off}.

10. Diffusion coefficient analysis. In the control experiment, we validated the 3D trajectory recorded by our system setup by comparing the theoretically predicted and experimentally estimated diffusion coefficient value of a bead freely diffusing in 90 wt % glycerol. The theoretically predicted diffusion coefficient D $(\mu m^2/s)$ is obtained by the Stokes-Einstein equation:

$$D = \frac{k_B T}{6\pi\eta r} \quad \text{Equation S10.1}$$

where k_B is the Boltzmann's constant $(1.38 \times 10^{-23}\ \mathrm{m^2 \cdot kg \cdot s^{-2} \cdot K^{-1}})$, T is the absolute temperature (K), η represents the dynamic viscosity $(0.1571\ \mathrm{N \cdot s \cdot m^{-2}})$, and r represents the radius of the spherical particle (10 nm). The diffusion coefficient *D* can also be obtained by the mean-squared-displacement (MSD) curve of the single-molecule trajectory. The MSD curve is defined as follows,

$$MSD(\tau) = \langle (\boldsymbol{r}(t+\tau) - \boldsymbol{r}(t))^2 \rangle \quad \text{Equation S10.2}$$

where τ represents the time lag, and $\boldsymbol{r}(t) = (\boldsymbol{x}(t), \boldsymbol{y}(t), \boldsymbol{z}(t))$ is the observed trajectory at time t. For normal diffusion in an isotropic medium, MSD is given by $MSD = 6D\tau$, where D is the diffusion coefficient. While within the complex environment of the cell, Brownian motion is affected by the obstacle, and thus the anomalous diffusion is introduced. In this case, MSD and diffusion coefficient is related by

$$MSD = 6D\tau^{\alpha} \quad \text{Equation S10.3}$$

where α is the diffusion exponent.

The MSD curve generally suffers from significant noise at longer time lag due to the fact that fewer data points cab be utilized to obtain the MSD. Thus, we fit only the first quarter of the MSD curve to quantify the diffusivity, *D*.

11. Fluorescence correlation spectroscopy (FCS) setup. FCS measurements were carried out with a confocal microscope. A pulsed laser (repetition rate 10 MHz) from PicoQuant LDH-P-C-640B was reflected by the dichroic mirror (Semrock FF650-Di01-25x36), and then focused by a 60X NA=1.2, water immersion objective (Olympus, UPLSAPO 60XW) to excite the Atto633 dyes. The fluorescence was collected by the same objective and filtered by ET700/75m (Chroma). An avalanche photodiode (APD, SPCM-AQ4C, Perkin-Elmer) was used to detect Atto633 dyes emission and a hardware correlator (ALV-7002 /EPP, ALV-GmbH) was used to compute autocorrelation functions. Unless otherwise noted, the laser excitation intensity was kept low (100 μW before entering the aperture of the objective) to avoid fluorescence saturation, triplet-state formation and photobleaching. The laser beam was focused 25 μm into the sample for all FCS measurements in this work.

12. FCS analysis. The one-component model is employed to fit the autocorrelation function $G(\tau)$ as follows,

$$G(\tau) = \frac{1}{N} g_d(\tau) X(\tau) \quad \text{Equation S12.1}$$

where τ represents the lag time, N is the average number of the molecules in the detection volume, $g_d(\tau)$ represents an autocorrelation function due to the translational diffusion, and $X(\tau)$ represents the fluctuation due to the fast-blinking kinetics. $g_d(\tau)$, and $X(\tau)$ are characterized as follows,

$$g_d(\tau) = \frac{1}{1+\left(\frac{\tau}{\tau_d}\right)^{\alpha}} \quad \text{Equation S12.2}$$

$$X(\tau) = 1 + \frac{Fe^{-\left(\frac{\tau}{\tau_T}\right)^{\beta}}}{1-F} \quad \text{Equation S12.3}$$

where, τ_d and τ_r represents the characteristic diffusion time and the mean triplet state relaxation time respectively, α and β are the anomalous factor and the stretch parameter individually, and F is the effective fraction of molecules in triplet states.

13. DNA model. The synthetic 5'-Atto633-labeled DNA oligomers and 5'-Iowa Black® FQ—labeled DNA oligomers with HPLC purified were purchased from Integrated DNA Technologies. The 8-bp dsDNA 87.5% GC content strand consists of the donor strand 5'-Atto633-TGGGCGGG-3' and the complementary strand 5'-Iowa Black® FQ-CCCGCCCA-3'; the 37.5% GC content strand consists of the donor strand 5'-Atto633- TGATTGTG-3' and the complementary strand 5'-Iowa Black® FQ-CACAATCA-3'. The phosphorothioate (PS) – modified 87.5% GC sequence consist of 5'-Atto633-T*GG*GC*GG*G-3', while the antisense strand is the same as 87.5% GC content strand. For all measurements, the samples are diluted to the appropriate concentration for single-molecule tracking.

14. Cell culture. HeLa cells were grown at 37℃ in a humidified atmosphere with 5% CO_2. Cells were maintained in DMEM/F12 medium (11320082, Thermo Fisher Scientific) supplemented with 10% heat-inactivated fetal bovine serum (16140071, Thermo Fisher Scientific) and 50 U/mL penicillin-streptomycin (15070063, Thermo Fisher Scientific). For chemical transfection, monolayer cells were seeded onto optical imaging 8-well Lab-Tek chambered coverglass (Cat. No. 154534, Thermo Scientific) with cell density 70–90% confluent per well. The cells were seeded a day before transfection. For the electroporation, 0.25% trypsin/EDTA solution (25200-056, Thermo Fisher Scientific) was used to release adherent cells.

15. Lipofection protocol. Cells were grown on 8-well Lab-Tek chambered coverglass (Cat. No. 154534, Thermo Scientific) for 24 hours in grown medium (70-90 % confluent at transfection). Transfection was carried out using Lipofectamine 3000 (Cat. No. L3000015, Thermo Scientific). Lipofectamine 3000 was diluted in Opti-MEM medium and mix well by vortexing 2-3 sec. Then, appropriate DNA concentration was diluted in Opti-MEM medium and mixed well with P3000™ reagent. After the diluted lipofectamine 3000 and DNA was mixed (1:1 ratio), the mixed solution was incubated for 10-15 minutes at room temperature and then added to the cell-adherent chambered coverglass. Transfection was carried out over 15 hours at 37°C.

16. Electroporation protocol. The adherent cells were released by the trypsin and centrifuge cells at 300g for 3 min. The cells were resuspended in the growth medium, and the numbers were measured by a hemocytometer. 10^6 cells and ssDNA (Probe: 10 nM; Target: 10, 100, 1000, 10000 nM) were transferred to the electroporation buffer (serum-free DMEM) in a 4 mm gap electroporation cuvette (BioRad) for 5 minutes at room temperature. Electroporation was carried out under different conditions (300 V, 125 μF; 200 V, 960 μF; 400 V, 25 μF) with infinite internal resistance value on the electroporation device (BioRad Gene Pulsar II). The cells were left for 10 minutes at room temperature. The cells were then seeded in growth medium on 8-well Lab-Tek chambered coverglass and allowed to recover for 8 hours.

17. Flow cytometry techniques. The cytotoxicity of electroporated HeLa cells was evaluated using a LIVE/DEAD® Viability/Cytotoxicity Assay Kit (Cat. No. L-3224, Thermo Scientific) obtained from Life Technologies (Supplementary Fig. 8). The kit is based on the use of two fluorescent probes, calcein AM, and Ethidium homodimer-1 (EthD-1). The live and dead cells were stained by calcein AM, and Ethidium homodimer-1 (EthD-1) that are sensitive to intracellular enzymatic activity and plasma membrane integrity, respectively.

18. Quantification of ssDNA in cell lysate by FCS. The ssDNA (5'-Atto633-TGGGCGGG-3') was delivered into live cells by electroporation as described before. Cell lysates were prepared using supplemented RIPA buffer (89901, Thermo Scientific) as protocol described and the Atto-labeled ssDNA concentrations were measured quantified FCS. In short, the electroporated cells were centrifuged at 300 g for 3 mins and washed by PBS. These steps are repeated three times. The supernatant was discarded and the weight of cells was measured by the equation.

$$\text{Cell weight (mg)} = (\text{empty microtube} + \text{cells}) - \text{empty microtube} \qquad \text{Equation S18.1}$$

And then, the Atto633-labeled ssDNA was extracted from live cells with adding 50 μL lysis buffer.

$$\text{Total weight of final sample (mg)} = (\text{empty microtube} + \text{cell lysate} + \text{lysis buffer}) - \text{empty microtube}$$

$$\text{Dilution times} = \frac{\text{total weight of final sample (mg)}}{\text{cell weight (mg)}} \qquad \text{Equation S18.2}$$

The mixture was gently pipetted up and down to suspend the cell pellet. The 50% pulse of sonication was to be used to increase yields. The mixture was then be gently shaken for 15 minutes on ice and centrifuged at 14000xg for 15 minutes to pellet the cell debris. The cell lysates with Atto633-labeled DNA were transferred to a new microtube for further analysis. The calibration curve of Atto633-labeled ssDNA in RIPA buffer has to be performed by FCS as the reference of the concentration of Atto633-labeled ssDNA. The average brightness of the specific concentration of Atto633-labeled can be obtained by FCS. The three parameters, number, resident time and single brightness of the ssDNAs in the detective volume, can also be obtained from the

autocorrelated curve fitting. The fitting formula is the same as the previous section. The average brightness from Atto633-labeled ssDNA in cell lysate was measured and analyzed by the equation.

$$\%\ \text{ssDNA in cell lysate} = \frac{\text{The concentration of Atto633-labeled ssDNA in cell lysates (nM)}}{\text{Atto633-labeled ssDNA concentration in solution before electroporation (nM)}} \quad \text{Equation S18.3}$$

19. High-resolution melting analysis.

2 µL of 100 µM single-stranded target DNA and 2 µL of 100 µM complementary DNA were added to the 16 µL Precision Melt Supermix®(which contains EvaGreen, Bio-Rad), achieving a final volume of 20 µL and a final DNA concentration of 10 µM. The acquisition was carried out in the SYBR channel and the acquired melting curves were analyzed using CFX Manager software (version 1.6, Bio-Rad). Before measurements, the samples were denatured at 93 °C for 1 min and cooled down to 4 °C for 30 min. During melting measurements, the temperature was increased from 4 to 100 °C in 0.2 °C incremental steps, with each step held for 5 s. Initially, the acquired fluorescence was plotted against melting temperatures (T_m). Normalization regions were selected before and after the major decrease in fluorescence.

$$RFU_{i,\ Normalized}(T) = \frac{RFU_i(T) - \min(RFU_i(T))}{\max(RFU_i(T)) - min(RFU_i(T))} \quad \text{Equation S19.1}$$

where i represents individual melting experiments.
The Gibbs energy ΔG was determined by the following,

$$\Delta G = -RT_m ln(K) \quad \text{Equation S19.2}$$

where R is the idea gas constant (1.99 cal/mol K), T_m represents the melting temperature, and K is the equilibrium constant (2/[ssDNA] in our case).

20. Quantification of DNA annealing/melting rate from ensemble measurement.
Assume we have a model:

$$\mathrm{R} + \mathrm{Q} \underset{k_{off}}{\overset{k_{on}}{\rightleftharpoons}} RQ \quad \text{Equation S20.1}$$

where R and Q represent reporter and quencher strand. The mathematical kinetics model for the above second-order reversible chemical reaction is

$$\frac{d[R]}{dt} = -k_{on}[R][Q] + k_{off}[RQ] \quad \text{Equation S20.2}$$

During the experiment, we will add quencher to the solution with reporter only. Therefore, the initial concentrations are $[R]_0$, $[Q]_0$, and $[RQ]_0$. Once reaction starts, the transient concentrations at time t become

$$[R] = [R]_0 - x(t) \quad \text{Equation S20.3}$$

$$[Q] = [Q]_0 - x(t) \quad \text{Equation S20.4}$$

$$[RQ] = [RQ]_0 + x(t) \quad \text{Equation S20.5}$$

The solution to the above differential equation is

$$x(t) = \frac{2\gamma\left(1 - e^{\sqrt{\beta^2 - 4\alpha\gamma}t}\right)}{\beta\left(1 - e^{\sqrt{\beta^2 - 4\alpha\gamma}t}\right) - \sqrt{\beta^2 - 4\alpha\gamma}\left(1 + e^{\sqrt{\beta^2 - 4\alpha\gamma}t}\right)} \quad \text{Equation S20.6}$$

where $\alpha = k_{on}$; $\beta = k_{on}([R]_0 + [Q]_0) + k_{off}$; and $\gamma = k_{on}[R]_0[Q]_0 - k_{off}[RQ]_0$.
Assume the fluorescence lifetime for reporter strand and the quenched-state is τ_1 and τ_2, respectively. The average lifetime value observed, τ, is as follows,

$$\tau = \frac{[R]}{[R]+[RQ]}\tau_1 + \frac{[RQ]}{[R]+[RQ]}\tau_2 = \frac{[R]_0\tau_1 + [RQ]_0\tau_2 + x(t)(\tau_2 - \tau_1)}{[R]_0 + [RQ]_0} \quad \text{Equation S20.7}$$

Equation S20.7 can be used to fit the ensemble lifetime traces acquired *in vitro* (Figure S24 B).

Table S1: Summary of measured DNA hybridization kinetics *in vitro*

Reporter strand concentration = 100 pM, Quencher strand concentration = 200 nM

	Sequence	$k'_{on}(s^{-1})$	$k_{off}(s^{-1})$
87.5% GC	TGGGCGGG	4.75 ± 1.16	9.61 ± 2.38
37.5% GC	TGATTGTG	4.50 ± 0.85	18.13 ± 3.09
PS_87.5% GC	T*GG*GC*GG*G	5.96 ± 1.18	10.76 ± 1.96

*Asterisk represents phosphorothioate modification.

Reporter strand concentration = 100 pM, Quencher strand concentration = 400 nM

	Sequence	$k'_{on}(s^{-1})$	$k_{off}(s^{-1})$
87.5% GC	TGGGCGGG	5.42 ± 1.30	8.01 ± 1.98
37.5% GC	TGATTGTG	4.77 ± 0.89	17.46 ± 2.98
PS_87.5% GC	T*GG*GC*GG*G	6.74 ± 1.31	9.16 ± 1.79

*Asterisk represents phosphorothioate modification

Reporter strand concentration = 100 pM, Quencher strand concentration = 600 nM

	Sequence	$k'_{on}(s^{-1})$	$k_{off}(s^{-1})$
87.5% GC	TGGGCGGG	6.36 ± 1.71	9.51 ± 2.44
37.5% GC	TGATTGTG	5.91 ± 0.98	17.49 ± 2.66
PS_87.5% GC	T*GG*GC*GG*G	7.23 ± 1.30	8.97 ± 1.57

*Asterisk represents phosphorothioate modification

Reporter strand concentration = 100 pM, Quencher strand concentration = 800 nM

	Sequence	$k'_{on}(s^{-1})$	$k_{off}(s^{-1})$
87.5% GC	TGGGCGGG	7.11 ± 1.50	7.57 ± 1.63
37.5% GC	TGATTGTG	6.02 ± 1.08	14.32 ± 2.32
PS_87.5% GC	T*GG*GC*GG*G	7.85 ± 1.41	7.90 ± 1.43

*Asterisk represents phosphorothioate modification

Reporter strand concentration = 100 pM, Quencher strand concentration = 1000 nM

	Sequence	$k'_{on}(s^{-1})$	$k_{off}(s^{-1})$
87.5% GC	TGGGCGGG	8.47 ± 1.58	8.12 ± 1.52
37.5% GC	TGATTGTG	7.58 ± 1.37	15.16 ± 2.79
PS_87.5% GC	T*GG*GC*GG*G	8.51 ± 1.66	7.25 ± 1.48

*Asterisk represents phosphorothioate modification

Table S2: Summary of measured DNA hybridization kinetics *in vivo*

Reporter strand concentration = 100** pM, Quencher strand concentration = 1.15** nM in HeLa cells after electroporation (characterized by FCS). Asterisk (**) means estimated concentration.

	Sequence	$k'_{on}(s^{-1})$	$k_{off}(s^{-1})$
87.5% GC (HeLa)	TGGGCGGG	5.37 ± 2.72	5.30 ± 1.60
37.5% GC (HeLa)	TGATTGTG	9.22 ± 7.77	11.52 ± 3.00
PS_87.5% GC (HeLa)	T*GG*GC*GG*G	10.36 ± 3.38	9.55 ± 3.14

*Asterisk represents phosphorothioate modification

Reporter strand concentration = 100** pM, Quencher strand concentration = 11.5** nM in HeLa cells after electroporation (characterized by FCS). Asterisks (**) means estimated concentration.

	Sequence	$k'_{on}(s^{-1})$	$k_{off}(s^{-1})$
87.5% GC (HeLa)	TGGGCGGG	10.48 ± 2.45	6.05 ± 5.74
37.5% GC (HeLa)	TGATTGTG	10.99 ± 1.22	10.00 ± 2.34
PS_87.5% GC (HeLa)	T*GG*GC*GG*G	10.81 ± 2.70	10.02 ± 3.21

*Asterisk represents phosphorothioate modification

Table S3: Summary of measured k_{on}, k_{off}, and K_a *in vitro* and *in vivo*

	$k_{on}(\times 10^6 M^{-1}s^{-1})$	$k_{off}(s^{-1})$	$K_a(\mu M^{-1})$
87.5% GC (Solution)	4.56 ± 0.54	8.56 ± 0.93	0.53 ± 0.09
37.5% GC (Solution)	3.71 ± 1.01	16.51 ± 1.67	0.22 ± 0.06
PS_87.5% GC (Solution)	3.11 ± 0.19	8.81 ± 1.34	0.35 ± 0.06
87.5% GC (HeLa)	491.50 ± 235.78	5.70 ± 0.38	86.23 ± 41.77
37.5% GC (HeLa)	170.50 ± 117.26	10.80 ± 1.67	15.79 ± 10.91
PS_87.5% GC (HeLa)	43.90 ± 151.44	9.79 ± 1.34	4.48 ± 15.47

Table S4: Summary of measured k_{on}, k_{off}, and K_a *in vitro* (ensemble measurement)

	$k_{on}(\times 10^6 M^{-1}s^{-1})$	$k_{off}(s^{-1})$	$K_a(\mu M^{-1})$
87.5% GC (Solution)	1.52 ± 0.09	0.11 ± 0.01	13.81 ± 1.67
37.5% GC (Solution)	0.60 ± 0.09	0.39 ± 0.07	1.55 ± 0.37
PS_87.5% GC (Solution)	0.35 ± 0.19	0.13 ± 0.02	2.78 ± 0.42

Table S5: Melting temperature and Gibbs energy for the 3 model DNA

	T_m (℃)	*ΔG (kcal/mol)*
87.5% GC (Solution)	34.8	-7.48
37.5% GC (Solution)	28.6	-7.33
PS_87.5% GC (Solution)	32.6	-7.43

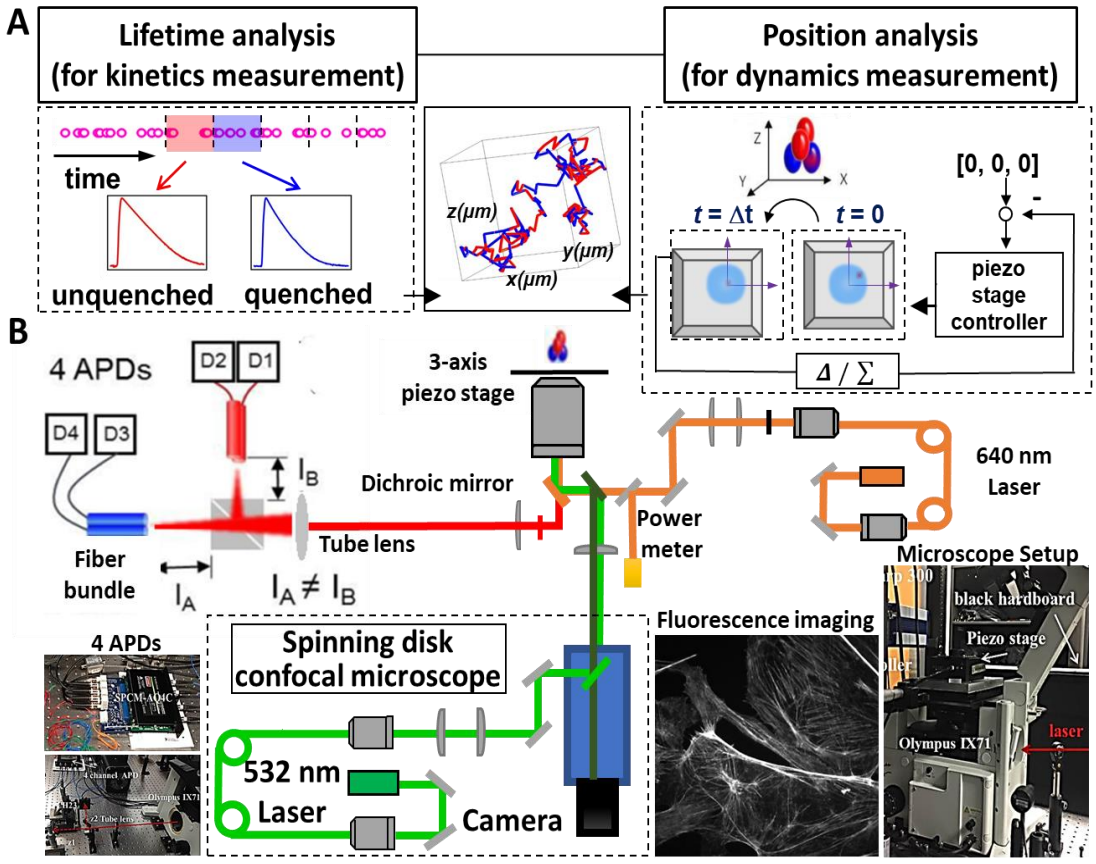

Figure S1 | Schematic of the confocal-feedback 3D single-molecule tracking (3D-SMT) system. (**A**) The 3D molecular trajectory is derived from the motion history of the xyz piezo stage (A, right). Using a TCSPC module, we are able to time tag the collected photons and eventually obtain a fluorescence lifetime trace of the tracked molecule (A, left). The lifetime trace can be merged with the molecule's 3D trajectory to provide spatiotemporally resolved binding (short lifetime, blue traces) and unbinding (long lifetime, red traces) states of the tracked molecule. (**B**) In our 3D-SMT system, four barely overlapped confocal volumes are created in the sample space (red and blue oval balls), each corresponding to the front ends of four multimode optical fibers that connect to four APDs. The two fiber bundles (red and blue) are orthogonally installed and slightly offset along the optical axis ($I_A \neq I_B$), giving the four confocal volumes a "tetrapod" geometry in the sample space. By comparing the differences in photon counts of the 4 detection channels, the 3D position of the tracked molecule is estimated. A feedback algorithm then drives the piezo stage to bring the molecule back to the center of confocal volumes. Thus, the motion history of the xyz piezo stage represents the 3D trajectory of the tracked molecule. By integrating a spinning disk unit (CrestOptics) with the 3D-SMT system (with Andor EMCCD camera), we could map the 3D trajectory of a reporter strand to the 3D volumetric image.

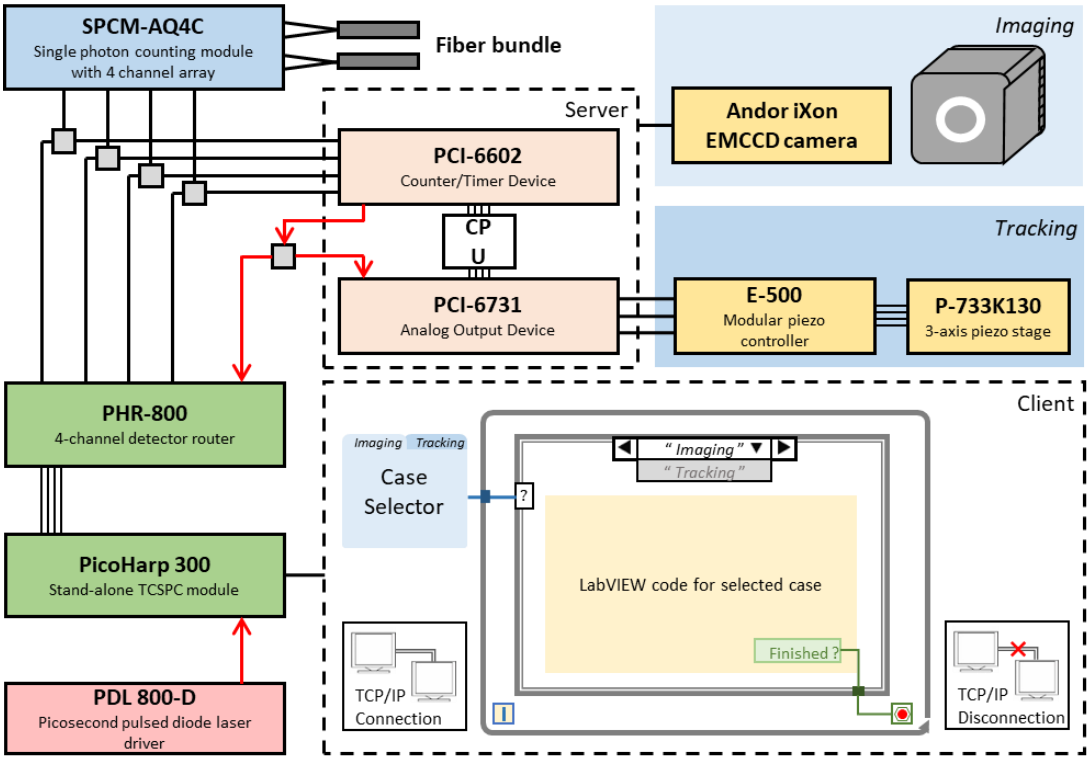

Figure S2 | Schematic of connection and LabVIEW control system. From our system layout, the SYNC OUTPUT of PDL 800-D picosecond pulsed diode laser drive is connected to the sync channel, CHANNEL 0, of PicoHarp 300. The detector router (PHR-800) is utilized to perform sophisticated and fast multidimensional fluorescence detection methods. In the client workstation (LabVIEW), we developed a user interface which allows us to select the experimental mode ("Imaging", "Tracking"). For "Imaging" mode, the TCP/IP connection between client and server is established in the beginning. Then we are able to control the Andor EMCCD camera to take cell images until we finish the experiment. In the end, the TCP/IP connection is disconnected. For "Tracking" mode, the TCP/IP connection is established first as well. Then we start the experiment and begin recording the number of photons in each channel of two optical fiber bundles every 5 ms. Based on the measurement, at the server workstation, an active feedback control algorithm is performed to drive the xyz piezo stage (P-733K130, PI) via the piezo controller (E-500) and keep the target molecule at the center of the confocal volumes. As the 3D trajectory of the molecule obtained upon the motion history of the piezo stage, our tracking range is ± 15 μm in all three dimensions (i.e. the travel range of the stage). In the meantime, at the client workstation, using a picosecond pulsed laser source and a time-correlated single photon counting (TCSPC) module with Time-Tagged Time-Resolved (TTTR) mode, we are able to measure the fluorescence lifetime of the tracked molecule. After finishing the experiment, the TCP/IP connection is disconnected, and the tracking history and the information of time tag and TCSPC time are saved at the client workstation.

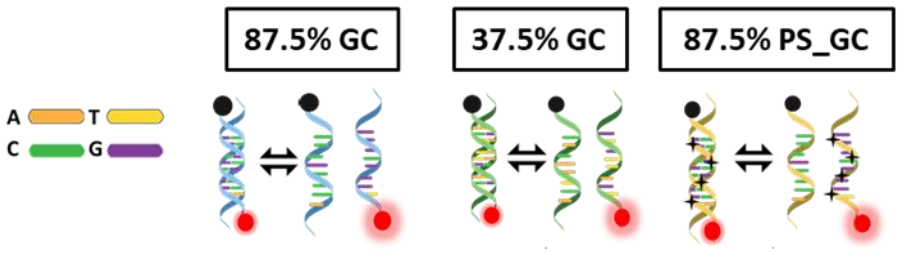

	Sequence 5′ → 3′
87.5% GC	/5Atto633/ TGGGCGGG (Reporter)
	/5IABkFQ/ CCCGCCCA (Quencher)
37.5% GC	/5Atto633/ TGATTGTG (Reporter)
	/5IABkFQ/ CACAATCA (Quencher)
87.5% PS_GC	/5Atto633/ T*GG*GC*GG*G (Reporter)
	/5IABkFQ/ CCCGCCCA (Quencher)

Figure S3 | Description of the 3 DNA models used for 3D-SMT *in vitro* and *in vivo*. In this work, we evaluated and compared the *in-vitro* and *in-vivo* kinetics of 3 reporter strands with different GC content and DNA modification. *Asterisk represents phosphorothioate modification.

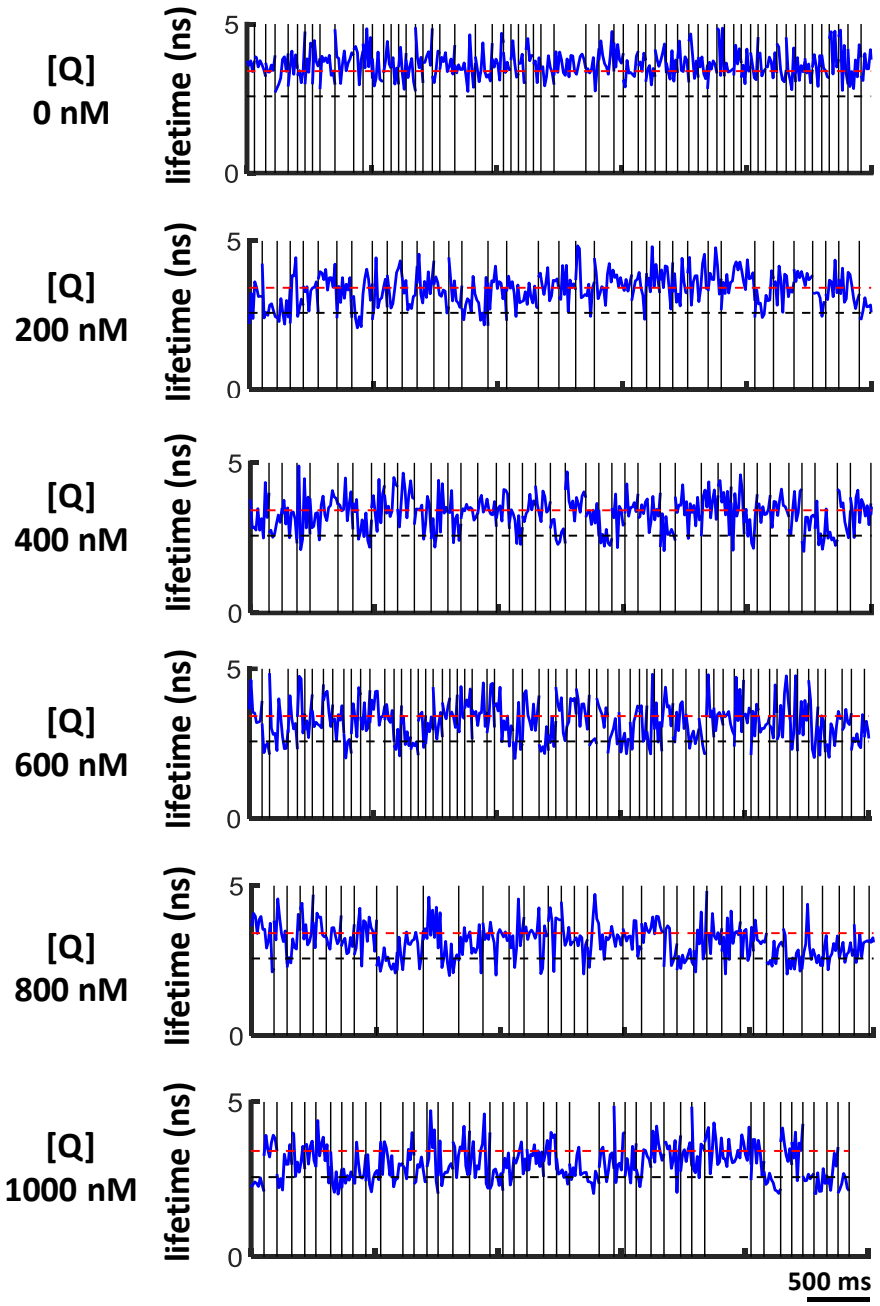

Figure S4 | Lifetime traces of 87.5% GC strand measured *in vitro* with different quencher strand concentrations. Red dashed line represents unbinding state (3.60 ns), and black dashed line represents binding state (2.61 ns). More binding states are observed as the concentration of quencher increases. This *in-vitro* experiment was carried out in the 70 wt% glycerol/20 mM Tris-HCl pH 8.0 solution. The temporal resolution of the lifetime traces is 15 ms.

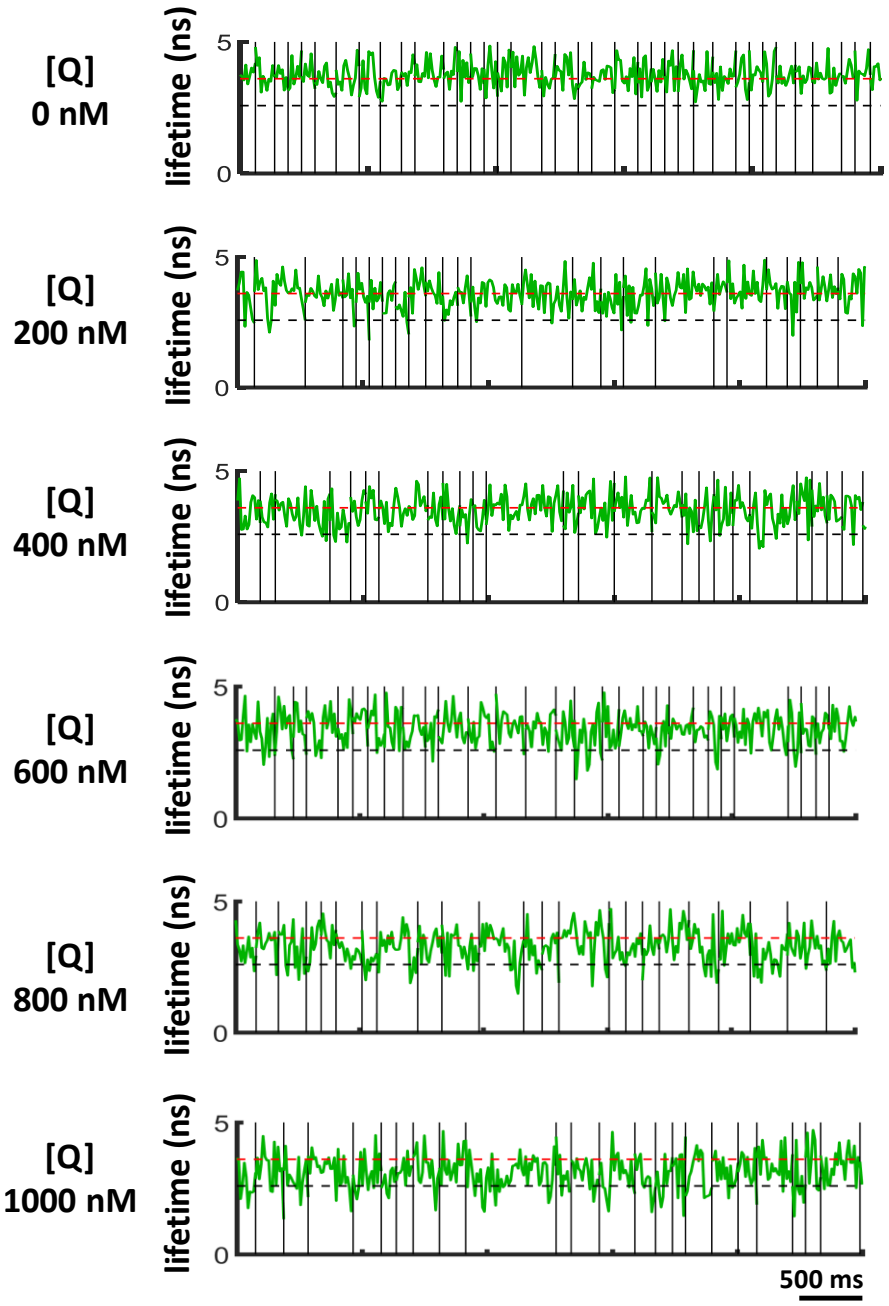

Figure S5 | Lifetime traces of 37.5% GC strand measured *in vitro* with different quencher strand concentrations. Red dashed line represents unbinding state (3.60 ns), and black dashed line represents binding state (2.59 ns). More binding states are observed as the concentration of quencher increases. This *in-vitro* experiment was carried out in the 70 wt% glycerol/20 mM Tris-HCl pH 8.0 solution. The temporal resolution of the lifetime traces is 15 ms.

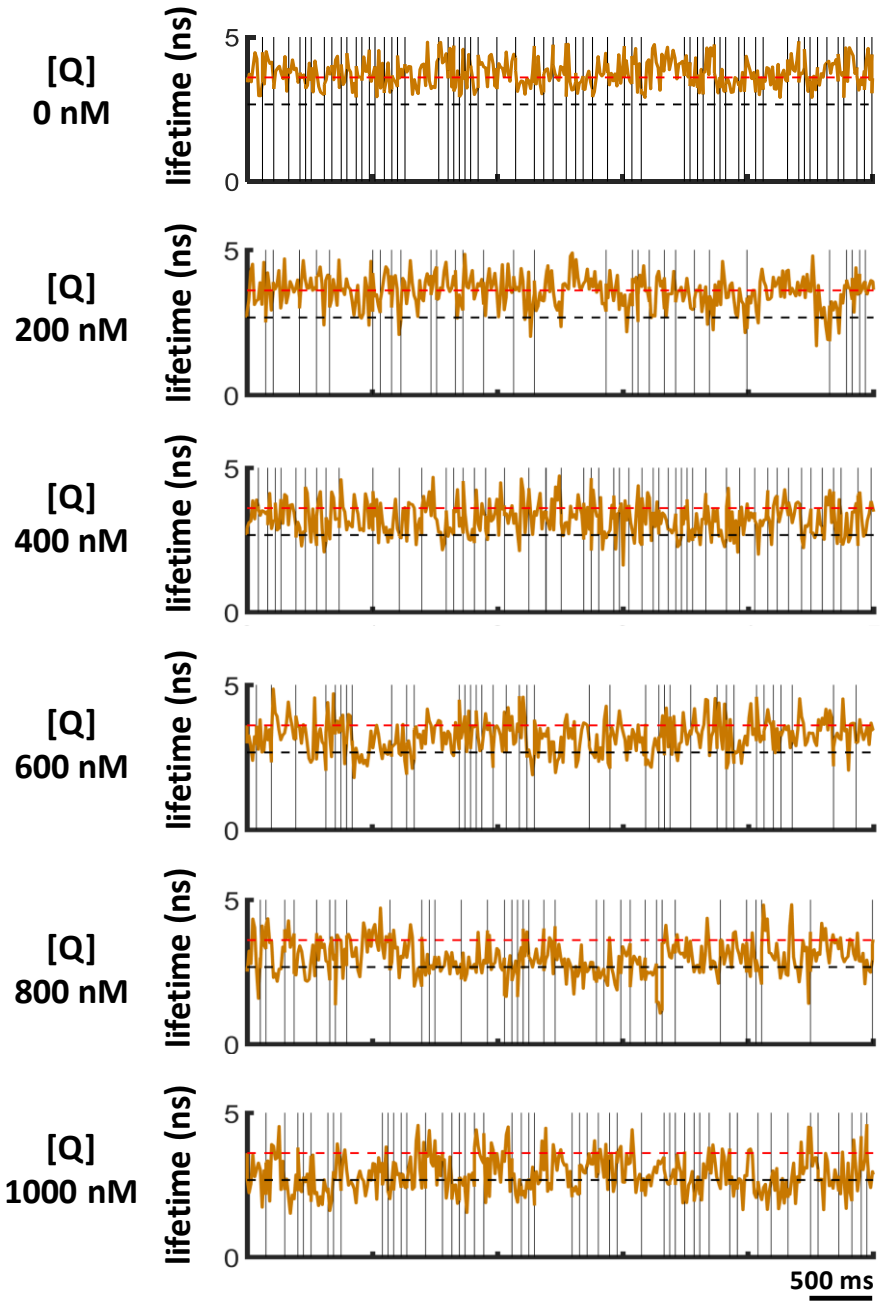

Figure S6 | Lifetime traces of 87.5% PS-GC strand measured *in vitro* with different quencher strand concentrations. Red dashed line represents unbinding state (3.60 ns), and black dashed line represents binding state (2.66 ns). More binding states are observed as the concentration of quencher increases. This *in-vitro* experiment was carried out in the 70 wt% glycerol/20 mM Tris-HCl pH 8.0 solution. The temporal resolution of the lifetime traces is 15 ms.

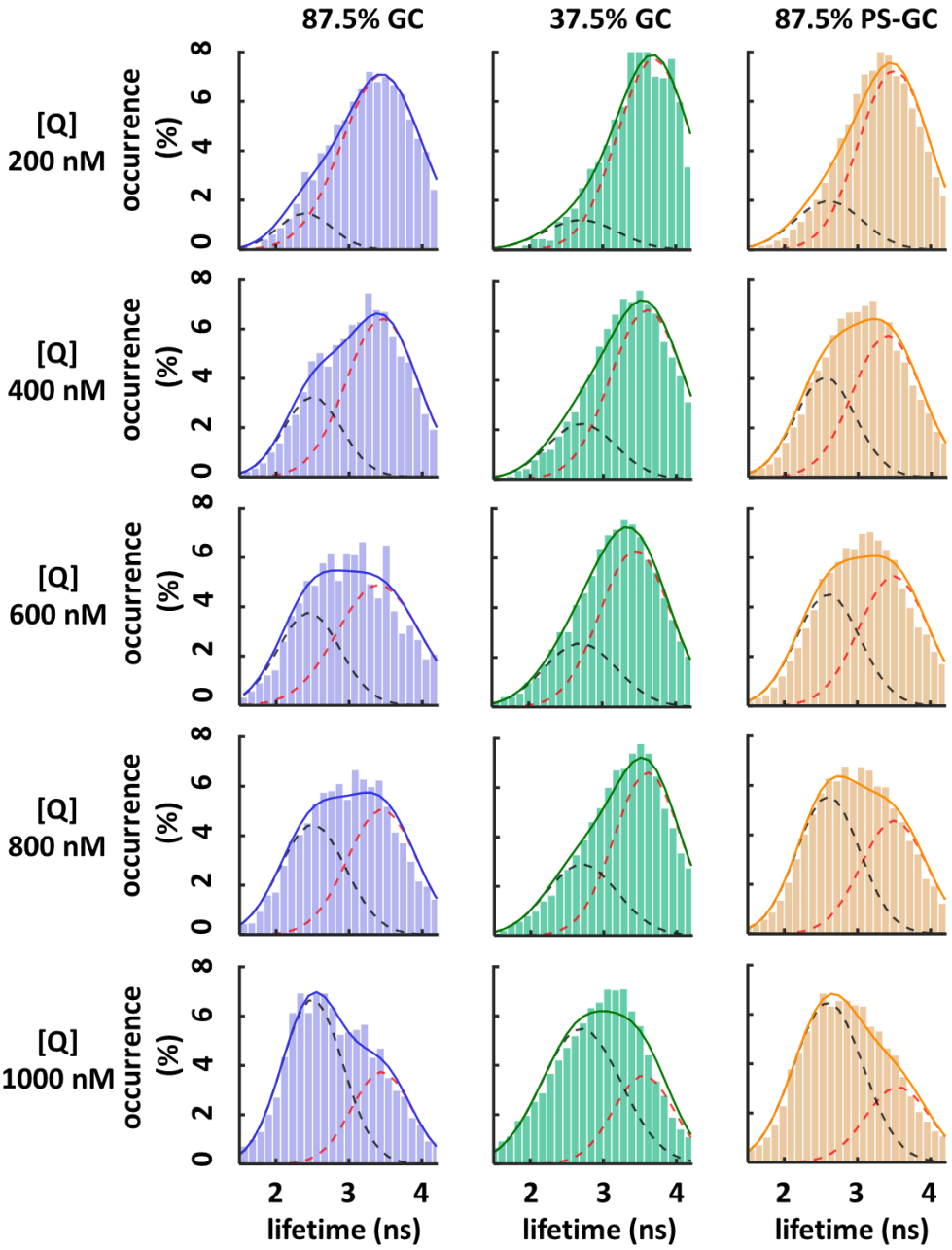

Figure S7 | Lifetime histograms built from the lifetime traces (*in vitro*). Histograms obtained from lifetime traces (**Figure. S4-S6**) clearly showed two states (~2.63 and ~3.60 ns) when quencher concentration increases from 200 -1000 nM, more binding state populations are observed. Red dashed line represents unbinding state, and black dashed line represents binding state. The distribution of the histogram transforms from negatively skewed into positively skewed as the quencher strand concentration increases.

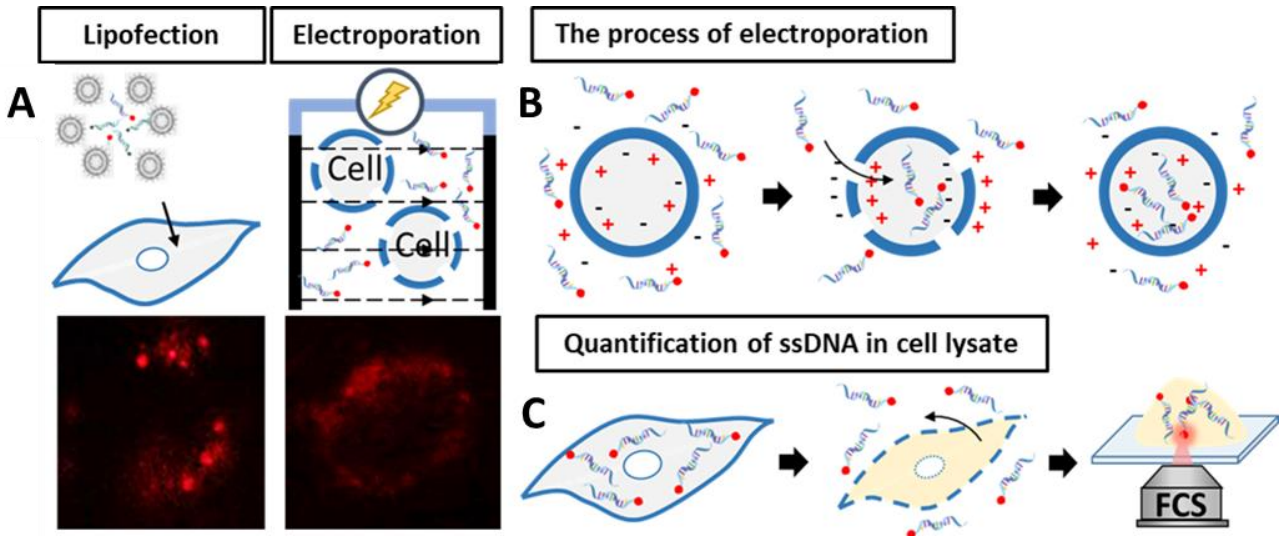

Figure S8 | Schematic of the DNA delivery and quantification of DNA concentration in cell lysate. (A) Delivery of DNA into live cells by lipofection and electroporation (B). In contrast to the reporter strands delivered by electroporation, the reporter strands delivered by lipofection were not evenly distributed. This suggested that the DNA strands were trapped and accumulated in distinct areas. Therefore DNA was introduced into live cells by electroporation in this article. (C) Cell lysates were prepared by RIPA buffer as protocol described and the Atto633-labeled ssDNA concentrations were quantified by FCS.

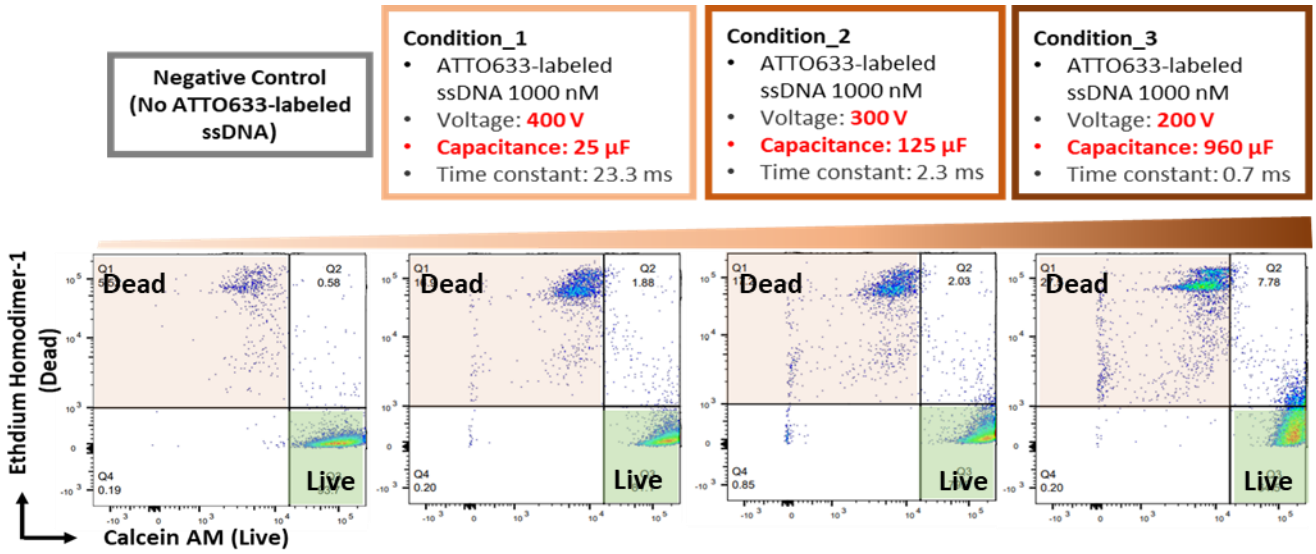

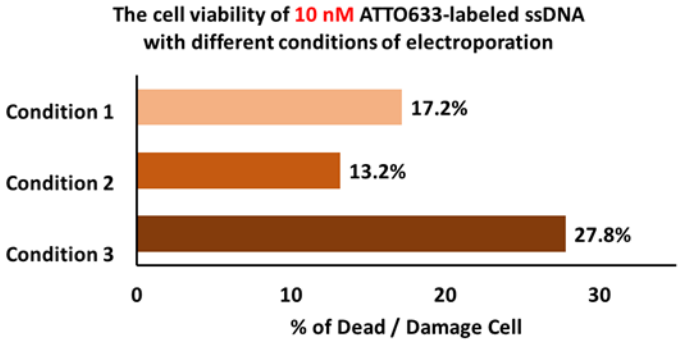

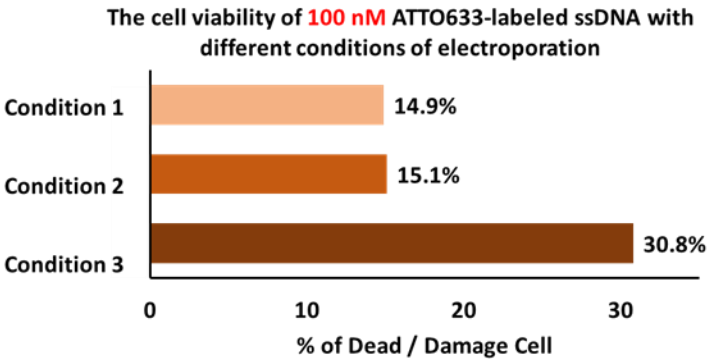

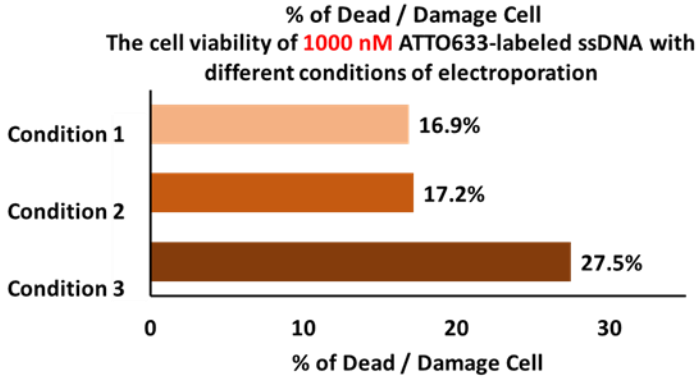

	Live Cells (%)	Dead Cells (%)
Negative Control	93.7	5.52
Probe(1000 nM)		
Condition 1	81.1	16.9
Condition 2	79.9	17.2
Condition 3	64.5	27.5
Probe(100 nM)		
Condition 1	82.7	14.9
Condition 2	82.6	15.1
Condition 3	59	30.8
Probe(10 nM)		
Condition 1	80.1	17.2
Condition 2	84.1	13.2
Condition 3	61.1	27.8

Figure S9 | Characterization of cell viability using LIVE/DEAD® Viability/Cytotoxicity Assay Kit and flow cytometry. LIVE/DEAD® Viability/Cytotoxicity Assay Kit allows us to identify the live and dead cells after electroporation (Condition 1:400 V, 25 μF; Condition 2: 300 V, 125 μF; Condition 3: 200 V, 960 μF). Calcein AM is a cell permeable probe, which is converted by intracellular esterase activity, ubiquitous in live mammalian cells, to green fluorescent (530 nm) calcein. Dead cells are stained by EthD-1 dye, which binds to cellular DNA of cells with their membrane compromised/permeabilized. The suspension electroporated cells were washed with phosphate buffer saline (PBS) three times and suspend in 1 mL PBS buffer. 2 μL of 50 μM calcein AM and 4 μL of 2 mM EthD-1 stock were added to each sample and incubated 20 min at room temperature protected from light before measurement. 1 mL stanning cells were transferred to the 5 mL BD Falcon™ Tubes and each tube was acquired using a BD LSR Fortessa cell analyzer. Calcein green fluorescence and EthD-1 red fluorescence emission were recorded using 530/30 and 610/20 band-pass filters, respectively. Live and dead control populations were also measured for proper live and dead populations discrimination and gating. Dead cells were obtained by inducing cell death with 70% ethanol solution. Forward and side scatter data were also collected to evaluate cell damage and morphology changes induced by electroporation. The percentage of electroporation induced cell death/damage was calculated based on the control cell population gating and manufacturer's instructions. The data was analyzed and plotted by FlowJo. Condition 2 was selected for electroporation.

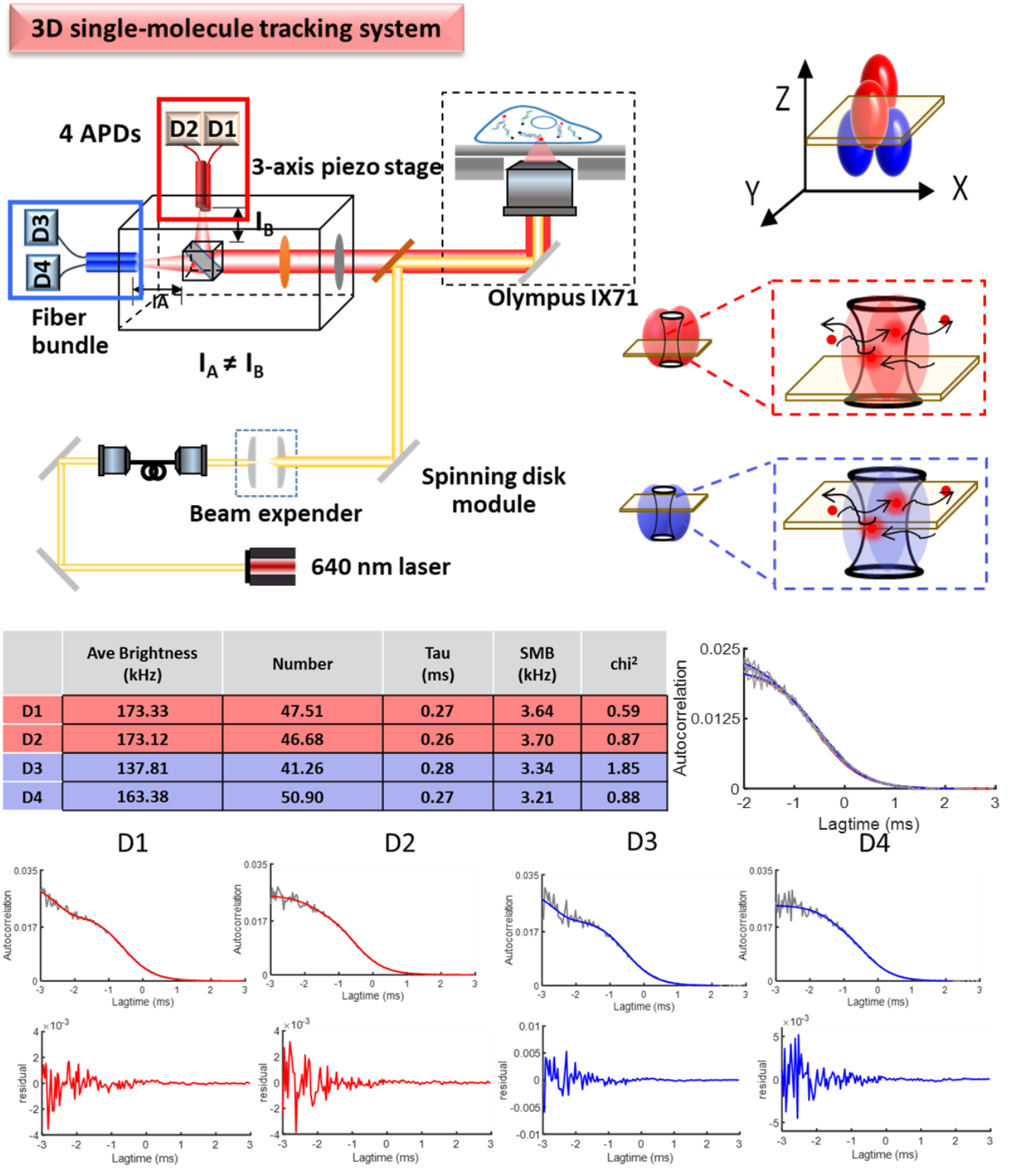

	Ave Brightness (kHz)	Number	Tau (ms)	SMB (kHz)	chi²
D1	173.33	47.51	0.27	3.64	0.59
D2	173.12	46.68	0.26	3.70	0.87
D3	137.81	41.26	0.28	3.34	1.85
D4	163.38	50.90	0.27	3.21	0.88

Figure S10 | Calibration of detection volume and single-molecule brightness by FCS. The four confocal volumes generated by the 50-μm core diameters pinhole, respectively, provide four detection volume. The setup concept is the same as fluorescence correlated spectroscopy (FCS), which can serve as the indicator of the brightness of single molecule and instrumental

calibration. Before the experiment is performed, the 10 nM Atto633-labeled ssDNA will be characterized by the overlapped confocal volumes. As the table and figures show, the single-molecule brightness (SMB) of Atto633-labeled ssDNA in DI water is around 3.5 kHz and the resident time (τ_D) is around 0.27 ms from each channel.

Calibration line of DNA in RIPA buffer

Solution	C_{DNA} (nM) In electroporated buffer	Ave Brightness (kHz)	Number	Tau (ms)	SMB (kHz)	chi²
RIPA buffer	100nM	612.79	287.32	0.44	2.13	2.4
RIPA buffer	50nM	277.71	110.69	0.4	2.51	1.46
RIPA buffer	10nM	70.15	24.97	0.41	2.81	1.78
RIPA buffer	5nM	37.72	14.16	0.44	2.66	1.2
RIPA buffer	1nM	8.24	3.2	0.40	2.58	1.63

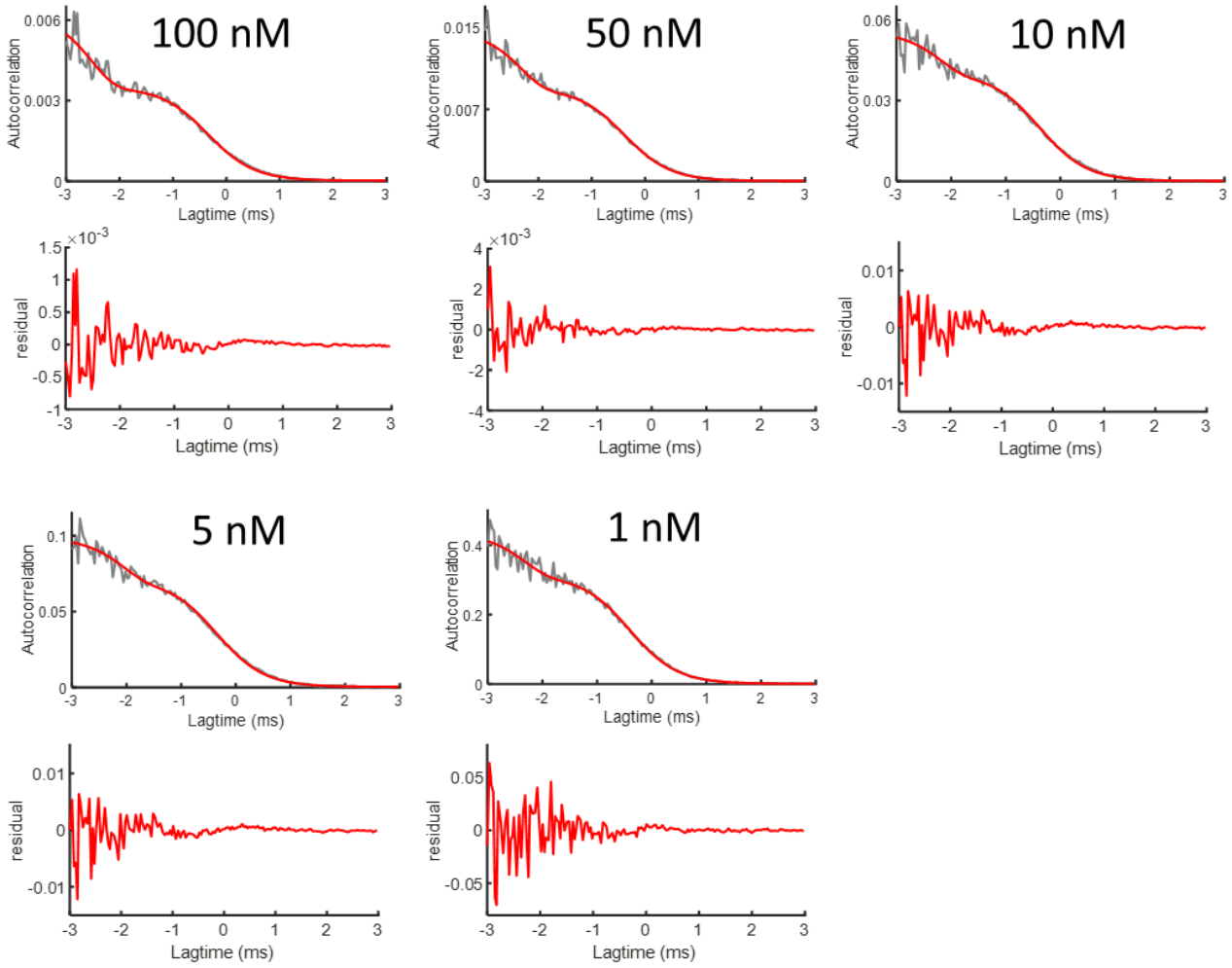

Figure S11 | Calibration line of Atte633-labeled ssDNA in RIPA buffer. As the table and figures show, the single-molecule brightness (SMB) of Atto633-labeled ssDNA in RIPA buffer is about 2.5-2.8 kHz and the resident time (τ_D) is around 0.42 ms from each channel.

The concentration of DNA in cell lysate

Solution		C_{DNA} (nM) Electroporated buffer	Ave Brightness (kHz)	Number	Tau (ms)	SMB (kHz)	chi²	C_{DNA} (nM) in diluted cell lysate	Dilution times	Estimated C_{DNA} (nM) Live HeLa cell
HeLa cell lysate	1	0 nM	0.89	x	x	x	x	X	x	x
HeLa cell lysate	2	10000 nM	981.94	514.2	0.58	1.91	1.38	x	x	x
HeLa cell lysate	3	1000 nM	169.73	72.2	0.66	2.35	2.14	28.28	6.21	175.62
HeLa cell lysate	4	500 nM	51.6	21	0.57	2.46	1.7	7.84	6.15	48.20
HeLa cell lysate	5	100 nM	14.17	6.53	0.66	2.17	5.02	1.73	8.25	14.29
HeLa cell lysate	6	50 nM	5.21	2.53	0.56	2.06	5.28	0.4	7.17	2.91
HeLa cell lysate	7	10 nM	1.8	1.33	0.6	1.35	4.87	X	x	x

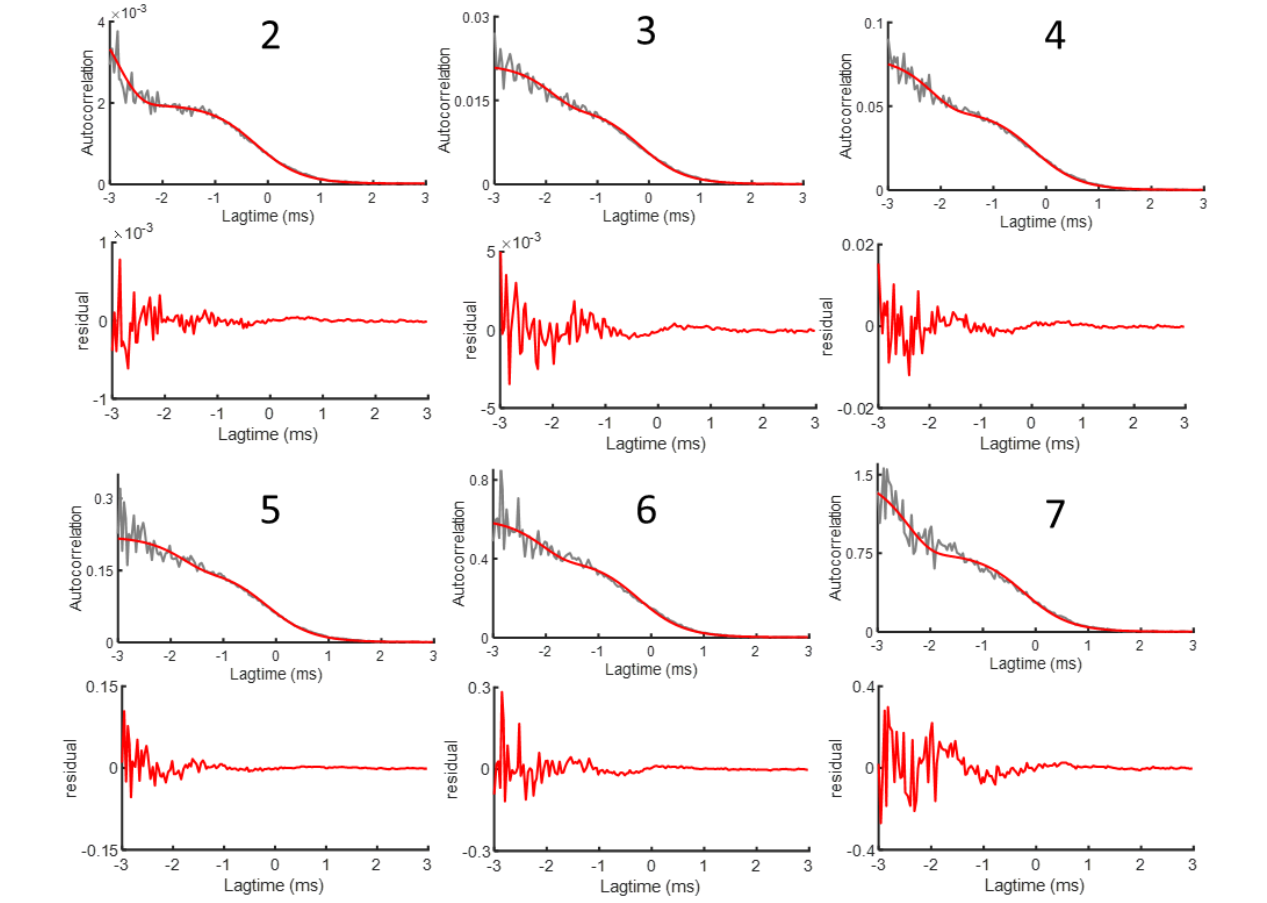

Figure S12 | Calibration line of Atte633-labeled ssDNA in cell lysate after electroporation. As the table and figures show, the single-molecule brightness (SMB) of Atto633-labeled ssDNA in cell lysate is about 2.3 kHz and the resident time (τ_D) is around 0.6 ms from each channel. Around 5-18% of Atto633-labeled ssDNA can be delivered into HeLa cells under 300 V, 125 μF.

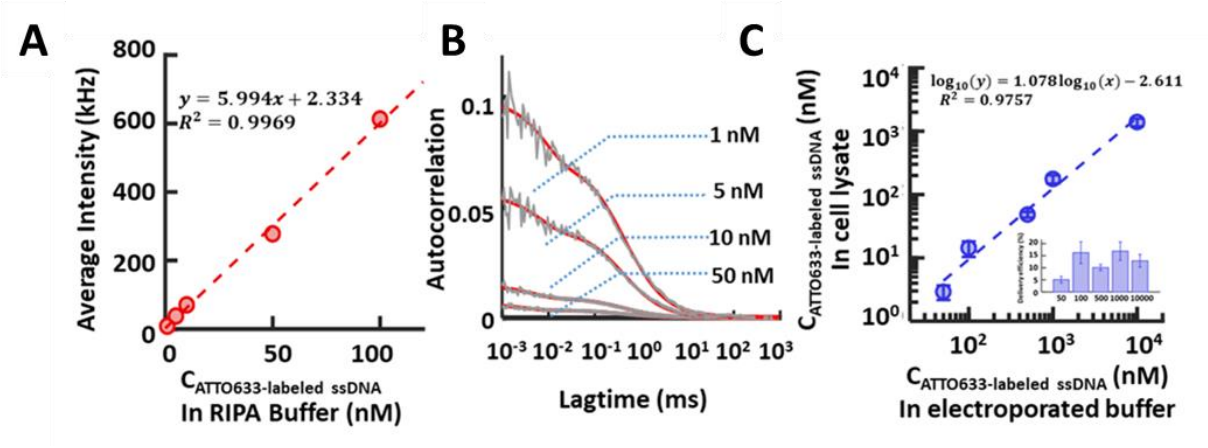

Figure S13 | **Quantification of DNA concentration in cell lysate.** (A) The calibration line for Atto633-labeled ssDNA in RIPA buffer. To build the calibration curve, we prepared our solution in ascending concentrations. The average intensity shows a highly linear dependence on the DNA concentration; the R^2 of the calibration curve performed in RIPA buffer is 0.99. (B) The autocorrelation curve corresponding to the data in (**A**). (**C**) The amount of DNA in cell lysate as a function of the DNA concentration in electroporation buffer. Inset in (C) shows the delivering efficiency with different concentration. Around 5-18% of Atto633-labeled ssDNA can be delivered into HeLa cells under 300 V, 125 μF.

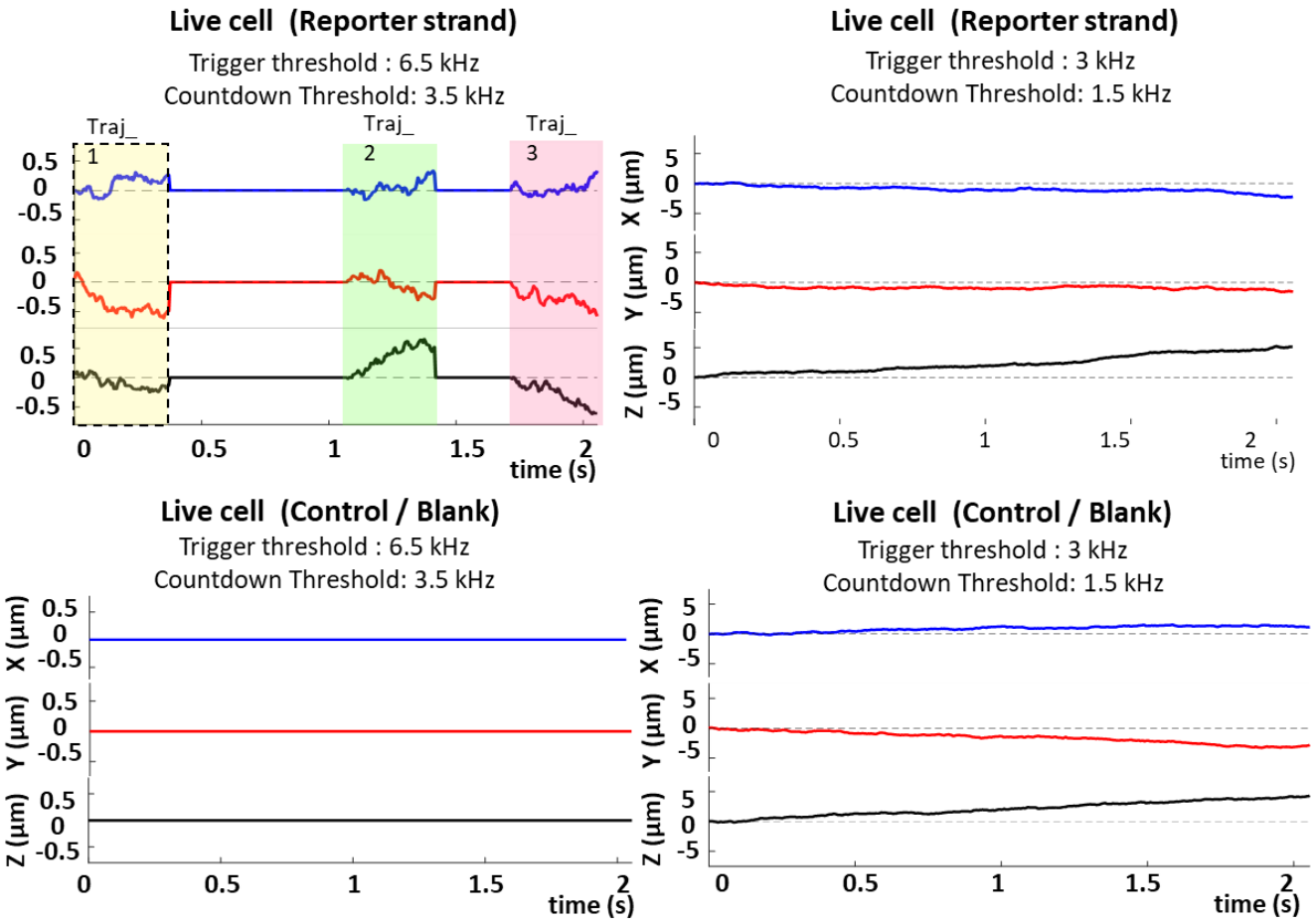

Figure S14 | Summary of the LabVIEW system threshold determination. The figure demonstrated that our system could actively track molecules that randomly walked into detection volume for hundreds of milliseconds. On the other hand, when the threshold was set too low (3 kHz, 1.5 kHz), the system is tacking the noise. Here the thresholds were set 6.5 and 3.5 kHz for intracellular tracking. It shows that ATTO633 dye is bright enough to overcome the background issue in *in-vivo* tracking.

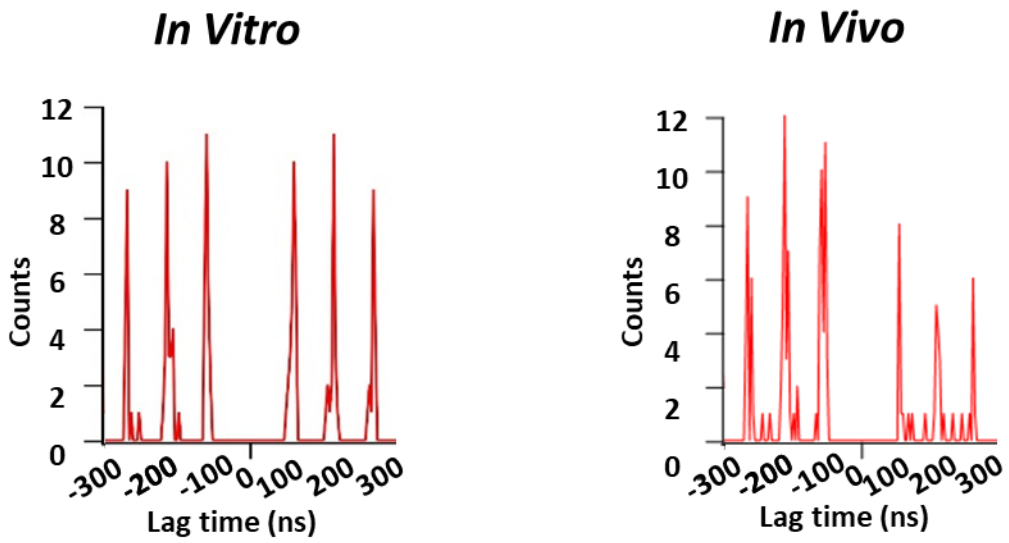

Figure S15 | Photon pair-correlation histogram for antibunching analysis. The dip at zero delay indicates that the probability of the tracked molecule emitting two photons simultaneously is nearly zero. The peaks in the histogram are equally spaced by 100 ns, identical to the repetition rate of the pulsed laser (10MHz). The experimental condition of *In Vitro* is 1X PBS + 70% Glycerol (100 pM ATTO633-labeled ssDNA) and *In Vivo* is in live HeLa cell (100** pM Atto633-labeled ssDNA in HeLa cells after electroporation). Asterisk (**) means estimated concentration.

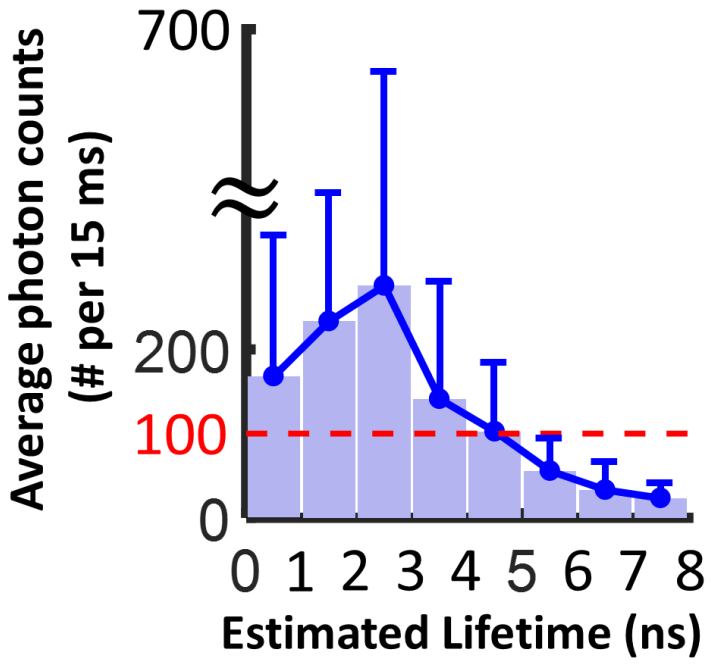

Figure S16 | Unexpectedly long lifetime (> 5 ns) was recorded when insufficient photons for lifetime fitting. Each bar shows the average number of photons utilized for MLE lifetime fitting which has a prediction between [0, 1], [1, 2], …, [7, 8]. 100 detected photons are demonstrated sufficient to determine a single exponential decay. The lifetime greater than 5 ns are estimated with insufficient photon counts (< 100).

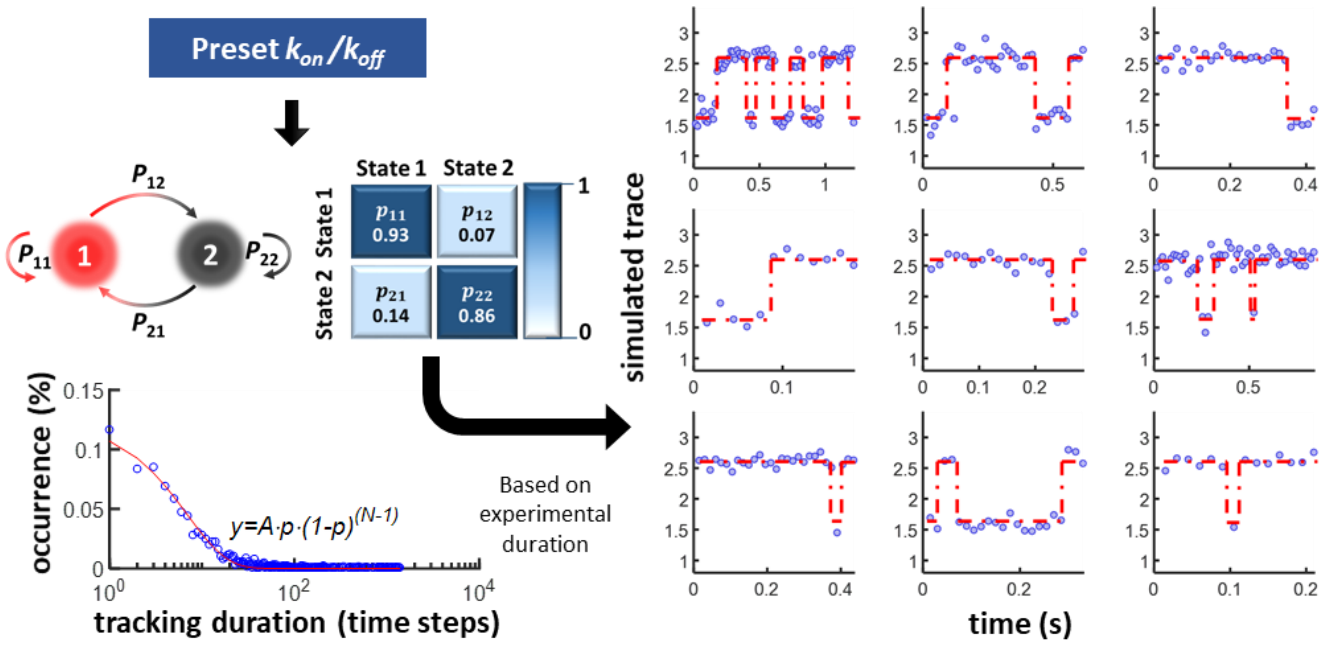

Figure S17 | Schematic of ebFRET analysis simulation. First, we would preselect the kinetic parameters (k_{on} = 5 s^{-1}, k_{off} = 10 s^{-1}), and thus obtained the transition probability matrix (p_{11} = 0.93, p_{12} = 0.07, p_{21} = 0.14, p_{22} = 0.86) for HMM process. In addition, according to the tracking duration from our experiments, the probability of losing track of the molecule in each time step was calculated (p = 0.17) via the model of Bernoulli trails. With the transition matrix and the probability of losing track, several simulated lifetime traces were generated for ebFRET analysis.

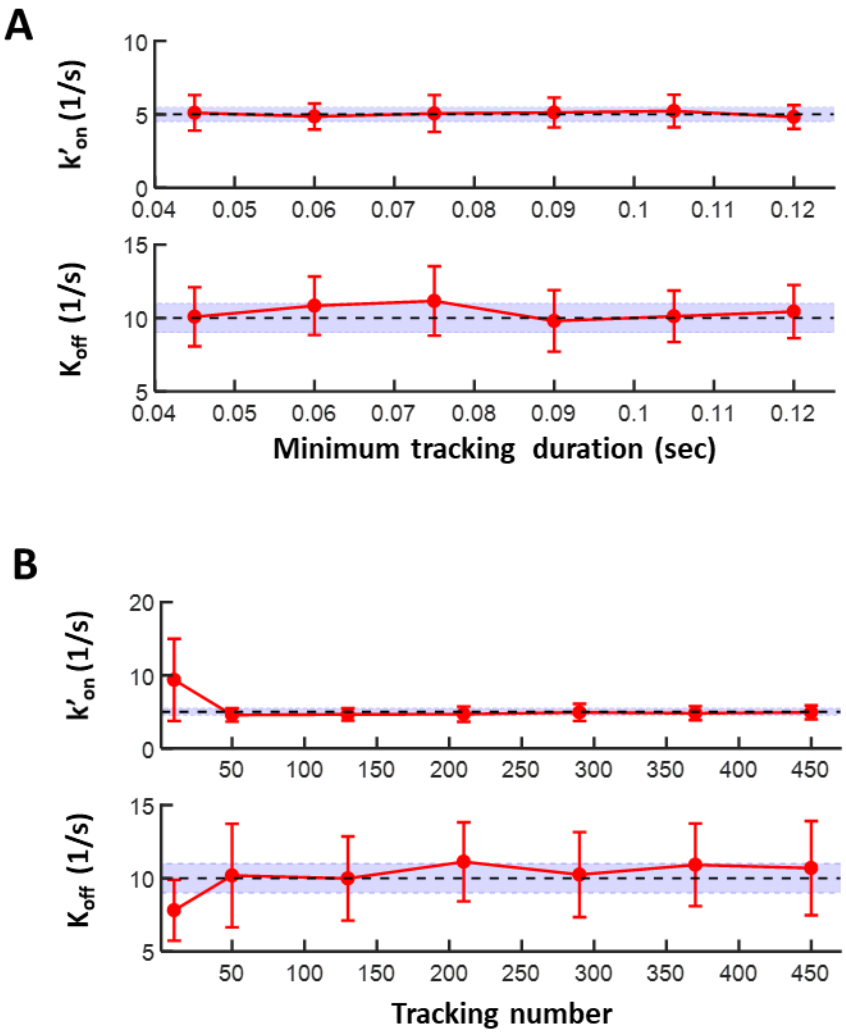

Figure S18 | **Simulation results with ebFRET analysis**. (A) From our simulated results, we plotted the estimated k'_{on}, k_{off} as a function of minimum tracking duration used for ebFRET analysis. Error bars denote the standard deviation. The black dotted line represents the true value. The blue area represents the range within 10% relative error. The relative error of the estimation is smaller than 10 % as long as the tracking duration is more than 0.45 sec. (B) From our simulated results, we plotted the estimated k'_{on}, k_{off} as a function of number of lifetime traces used for ebFRET analysis. Error bars denote the standard deviation. The black dotted line represents the true value. The blue area represents the range within 10% relative error. The relative error of the estimation is smaller than 10 % as long as the number of the traces available is more than 50.

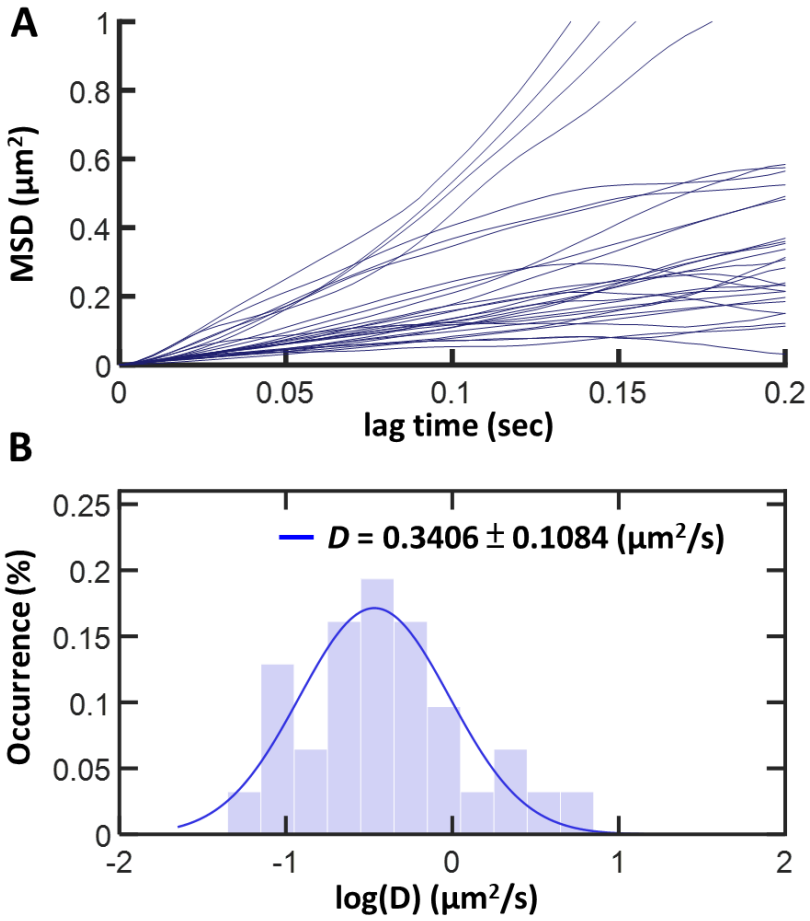

Figure S19 | Diffusivity analysis for representative trajectory for 87.5% GC. (A) Ensemble-averaged Mean-squared-displacement curves derived from the *in-vivo* trajectories with different quencher strand concentration (87.5 % GC). (B) Normalized histograms of experimentally derived dynamic parameters log(D), logarithm of the diffusion coefficients, is provided. The mean and standard deviation of the diffusion coefficients from the curve fitting are 0.34 ± 0.11 ($\mu m^2/s$).

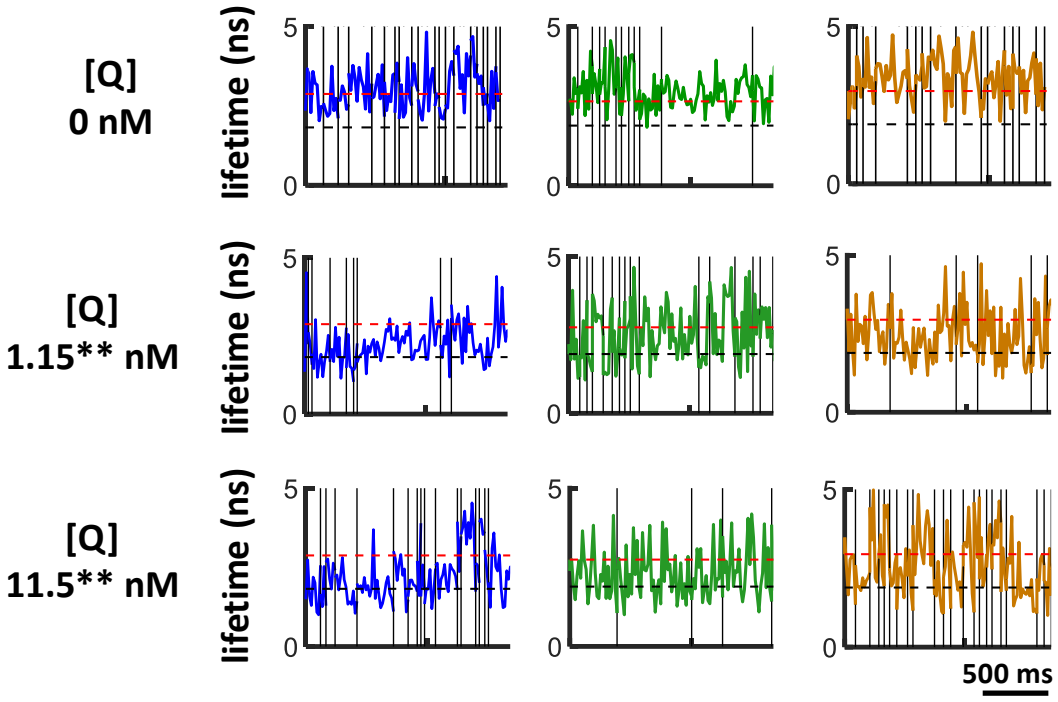

Figure S20 | **Lifetime traces measured *in vivo* with different quencher strand concentration** (blue, 87.5 % GC; green, 37.5 % GC; orange, 87.5 % PS-GC). Red dashed line represents unbinding state (2.71 ns), and black dashed line represents binding state (1.81 ns). More binding states are observed as the concentration of quencher increases. Asterisk (**) means estimated concentration characterized by FCS. These *in-vivo* experiments were carried out in live HeLa cells. The temporal resolution of the lifetime traces is 15 ms.

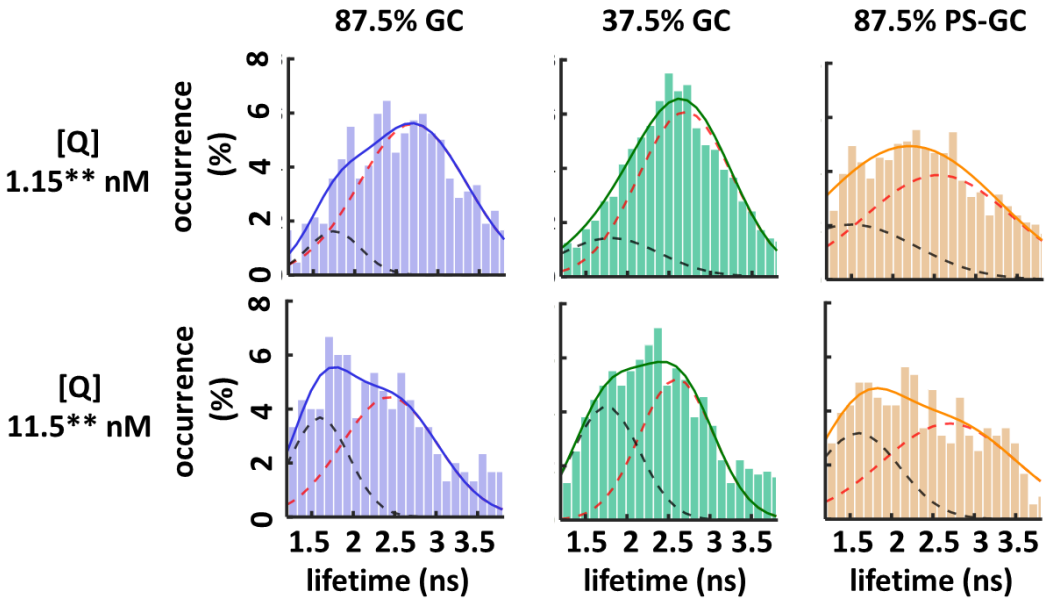

Figure S21 | Lifetime histograms built from the lifetime trace (*in vivo*). Histograms derived from (**Supplementary Fig. 18**) shows two states (~1.89 and ~2.71 ns) with different DNA sequences (87.5% GC, 37.5% GC, 87.5% PS-GC) and with different quencher strand concentration (1.15** nM – 11.5** nM). Red dashed line represents unbinding state, and black dashed line represents binding state. The distribution of the histograms transform from negatively skewed into positively skewed as the quencher strand concentration increases. Asterisk (**) means estimated concentration characterized by FCS.

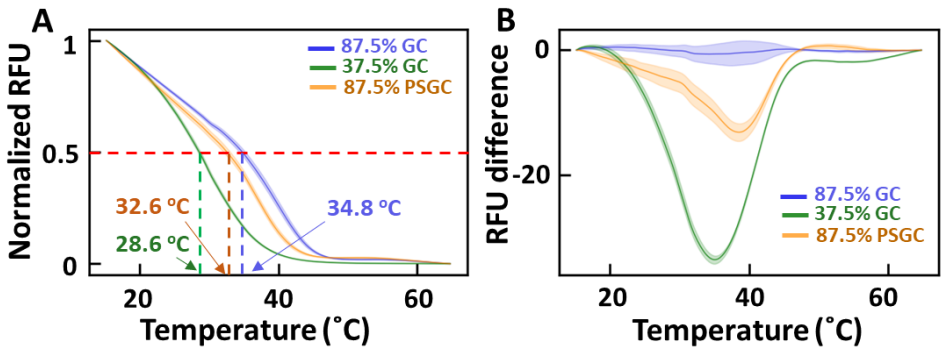

Figure S22 | High-resolution DNA melting curve analysis for the 3 model DNA strands. (a) Normalized melting curves for the 3 model DNA (5 replicates for each sample). (b) Differences plot using the melting curve of 87.5% GC strand as reference. Error bars (represented by ribbons) show standard deviations from five trials.

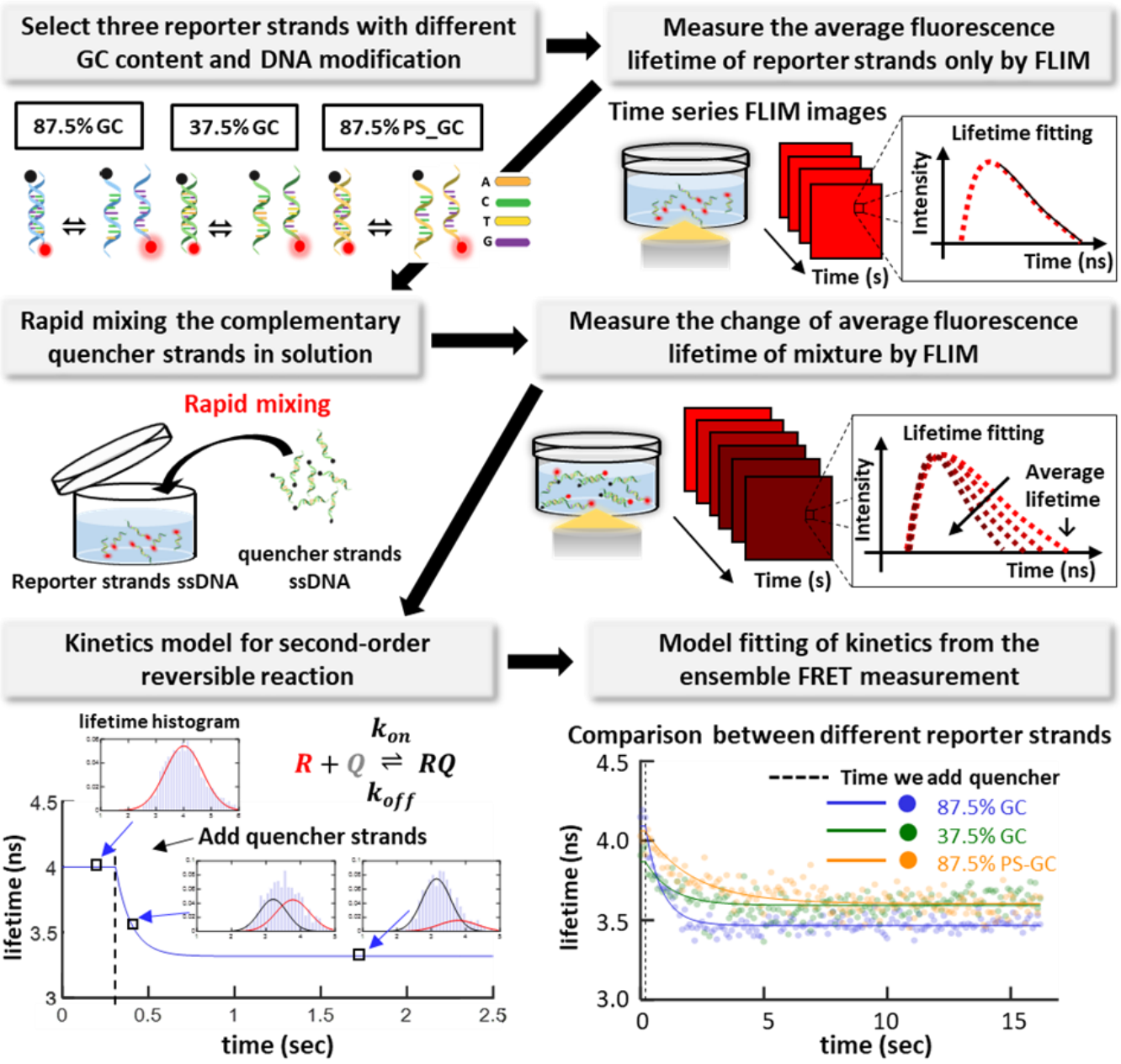

Figure S23 | Schematic of experimental design and data processing for *in-vitro* hybridization kinetics ensemble measurement. To investigate DNA hybridization kinetics with ensemble methods, we first selected three Atto633-labeled reporter strands with different GC content and DNA modification (87.5% GC, 37.5% GC, 87.5% PS-GC). Then we measured the average fluorescence lifetime of reporter strands only by fluorescence lifetime imaging microscopy (FLIM). After 300 ms, we performed rapid mixing with the complementary quencher strands in solution and measured the change of average fluorescence lifetime by FLIM simultaneously. To process the raw data from the above experiments, we derived a kinetics model based on the second-order reversible reaction and employed the proposed model to fit the observations.

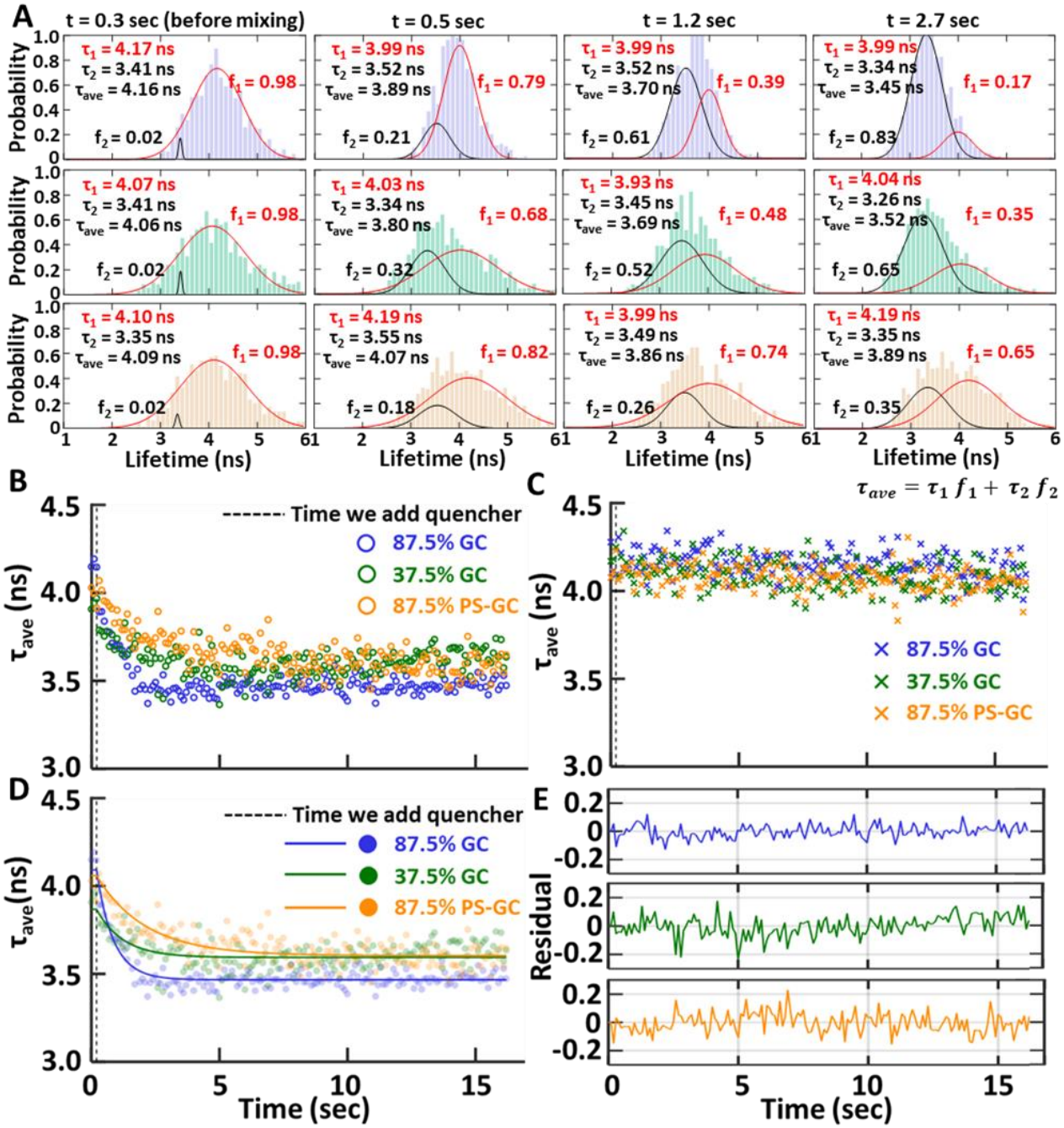

Figure S24 | Results for ensemble hybridization kinetics measurement *in vitro*. (A) Histograms of the average lifetime found in each pixel (totally 32×32 pixels). The two-component lifetime fitting results (τ_1: unquenched state, ssDNA; (τ_2: quenched state, dsDNA) and the corresponding fractions (f_1 and f_2) are shown in each subplot, where $\tau_{ave} = \tau_1 f_1 + \tau_2 f_2$. Red lines represent the population of the unquenched state (ssDNA), while black lines represent the quenched state (dsDNA). It is clear to see that the fraction of quenched state (f_2) increased while the average lifetime decreased, suggesting the formation of more dsDNA. (B) With quencher strands, the average lifetime decreased with time and reached a plateau. (C) Without quencher strands, the lifetime remained the same. (D) The τ_{ave} data points were fit with equation S20.7 (where τ_1, τ_2, $[R]_0$ and $[Q]_0$ were fixed and $[RQ]_0 = 0$ M) to extract k_{on} and k_{off}. (E) Residual of the fitting.

Reference

1. Grußmayer, K. S.; Herten, D.-P., Photon antibunching in single molecule fluorescence spectroscopy. In *Advanced Photon Counting*, Springer: 2014; pp 159-190.
2. van de Meent, J.-W.; Bronson, J. E.; Wiggins, C. H.; Gonzalez Jr, R. L., Empirical Bayes methods enable advanced population-level analyses of single-molecule FRET experiments. *Biophysical Journal* **2014,** *106* (6), 1327-1337.
3. Woodside, M. T.; Anthony, P. C.; Behnke-Parks, W. M.; Larizadeh, K.; Herschlag, D.; Block, S. M., Direct measurement of the full, sequence-dependent folding landscape of a nucleic acid. *Science* **2006,** *314* (5801), 1001-1004.
4. Peterson, A. W.; Heaton, R. J.; Georgiadis, R. M., The effect of surface probe density on DNA hybridization. *Nucleic Acids Research* **2001,** *29* (24), 5163-5168.
5. Bielec, K.; Sozanski, K.; Seynen, M.; Dziekan, Z.; ten Wolde, P. R.; Holyst, R., Kinetics and equilibrium constants of oligonucleotides at low concentrations. Hybridization and melting study. *Physical Chemistry Chemical Physics* **2019,** *21* (20), 10798-10807.
6. Heaton, R. J.; Peterson, A. W.; Georgiadis, R. M., Electrostatic surface plasmon resonance: Direct electric field-induced hybridization and denaturation in monolayer nucleic acid films and label-free discrimination of base mismatches. *Proceedings of the National Academy of Science* **2001,** *98* (7), 3701-3704.
7. Wong, I. Y.; Melosh, N. A., Directed Hybridization and Melting of DNA Linkers using Counterion-Screened Electric Fields. *Nano Letters* **2009,** *9* (10), 3521-3526.
8. Kastantin, M.; Schwartz, D. K., DNA Hairpin Stabilization on a Hydrophobic Surface. *Small* **2013,** *9* (6), 933-941.
9. Watkins, H. M.; Vallee-Belisle, A.; Ricci, F.; Makarov, D. E.; Plaxco, K. W., Entropic and Electrostatic Effects on the Folding Free Energy of a Surface-Attached Biomolecule: An Experimental and Theoretical Study. *Journal of the American Chemical Society* **2012,** *134* (4), 2120-2126.
10. Peterson, E. M.; Manhart, M. W.; Harris, J. M., Single-Molecule Fluorescence Imaging of Interfacial DNA Hybridization Kinetics at Selective Capture Surfaces. *Analytical Chemistry* **2016,** *88* (2), 1345-1354.
11. Alberty, R. A.; Hammes, G. G., Application of the theory of diffusion-controlled reactions to enzyme kinetics. *The Journal of Physical Chemistry* **1958,** *62* (2), 154-159.
12. Dupuis, N. F.; Holmstrom, E. D.; Nesbitt, D. J., Single-molecule kinetics reveal cation-promoted DNA duplex formation through ordering of single-stranded helices. *Biophysical Journal* **2013,** *105* (3), 756-766.
13. Jungmann, R.; Steinhauer, C.; Scheible, M.; Kuzyk, A.; Tinnefeld, P.; Simmel, F. C., Single-molecule kinetics and super-resolution microscopy by fluorescence imaging of transient binding on DNA origami. *Nano Letters* **2010,** *10* (11), 4756-4761.